TIME-DEPENDENT EFFECTS IN MAGNETIC NANO PARTICLES

THESIS SUBMITTED FOR THE DEGREE OF
DOCTOR OF PHILOSOPHY (SCIENCE)
OF THE
WEST BENGAL UNIVERSITY OF TECHNOLOGY

SUVANKAR CHAKRAVERTY
SATYENDRANATH BOSE NATIONAL CENTRE
FOR BASIC SCIENCES
JD BLOCK, SECTOR 3, SALT LAKE CITY
KOLKATA 700 098, INDIA

MARCH, 2006

Aknowledgement

The word "Acknowledgement" is not enough for some of my senior teachers, colleagues and collaborators like Prof. Binayak Duttaray of S.N. Bose National centre for Basic Sciences (SNBNCBS), Prof. Aviad Frydman of Bar Ilan University, Dr. P. A. Sreeram of SNBNCBS and my supervisor Prof. Sushanta Dattagupta. Prof. Duttaray constantly helped me to understand the basic concepts of physics not only related to my Ph.D work but of all kinds. I enjoyed his company during my Ph.D. tenure not only as a teacher but also as a friend. He never felt inpatient of my stupid questions, rather he addressed them very patiently. His active support helped me to finish my Thesis. I did most of my experimental works with Prof. Aviad Frydman in his laboratory at Bar Ilan University, Israel. He never discouraged me to perform any kind of new measurement protocols even in his expansive and sophisticated instruments. I felt at home during my visit to his laboratory because of his warm hospitality. I am really grateful to Dr. P. A. Sreeram for his constant support and encouragement. His approach and dedication to physics encouraged me a lot. Prof. Sushanta Dattagupta is not only my formal Ph.D. supervisor, but he changed my vision to the real life. He constantly supported me not only academically but also mentally throughout my Ph.D. period. I always feel surprised to see how simply he explains very complicated physics. His illuminated course on "Non Equilibrium Statistical Mechanics" actually inspired me to study the relaxation dynamics of nanomagnetic particles. I owe this Thesis to them and my family.

I am grateful to Dr. S. Kumar of Jadavpur University for always giving me the preference of doing the Mössbauer experiment in the laboratory at University of Calcutta. Many discussions on Mössbauer study with him and his student as well as my friend Mr. B. Ghosh helped me a lot to clear up my ideas on the subject.

I am grateful to Dr. S. Sengupta of SNBNCBS, Prof. M.K. Sanyal of Saha Institute of Nuclera Physcis (SINP) and Prof. S. Sen of SINP, for their comments and suggestions on my work.

Finally I would like thank my dear friends like Mukul, Malay and Sudipta, who always encouraged me. They actively helped me to finish this Thesis. Their cordial feeling for me made my Ph.D. period most enjoyable.

List of publications:

1. **Size-dependent magnetic properties of $Mn_{0.5}Zn_{0.5}Fe_2O_4$ nanoparticles in SiO_2 matrix**, K. Mandal, S. Chakraverty, S. Pan Mandal, P. Agudo, M. Pal, and D.Chakravorty, **J. Appl. Phys. 92, 501 (2002)**

2. **Magnetic Properties of $NiFe_2O_4$ Nanoparticles in SiO_2 Matrix**, Suvankar Chakraverty, Kalyan Mandal, Subarna Mitra, Sanjay Chattopadhyay and Sanjay Kumar, **Japanese Journal of Applied Physics Vol. 43, No. 11A, 2004, pp.7782-7787 : (T01,C01)**

3. **Magnetic properties of $NiFe_2O_4$-SiO_2 nanocomposite**, S.Chakraverty et.al, **IJP 78A(2),177-183(2004)**

4. **Positron annihilation studies of some anomalous features of $NiFe_2O_4$ nanocrystals grown in SiO_2**, S. Chakraverty, Subarna Mitra, K. Mandal, P. M. G. Nambissan, and S. Chattopadhyayhys. **Phys. Rev. B, Vol. 71, page 024115 (2005)**

5. **Memory in a magnetic nanoparticle system: Polydispersity and interaction effects**, S. Chakraverty, M. Bandyopadhyay, S. Chatterjee, S. Dattagupta, A. Frydman, S. Sengupta, and P. A. Sreeram, **Phys. Rev. B, vol. 71, page 054401 (2005)**

6. **Effect of a weak ferromagnetic matrix on superparamagnetic behavior of a system of nanomagnetic particles**, S.Chakraverty, A. Frydman, Pol,V.G. et al (submitted).

7. **Magnetic Coding in a System of Nano-magnetic Particles** S.Chakraverty, A. Frydman, B. Ghosh, S. Kumar, **Applied Physics Letter, 88 , 042501 (2006)**

8. **"Stochastic Modeling of Coercivity " - A Measure of Non-equilibrium State**, S. Chakraverty,M. Bandyopadhyay (submitted)

9. **Memory in a magnetic nanoparticle system: Polydispersity and interaction effects**, S. Chakraverty, M. Bandyopadhyay, S. Chatterjee, S. Dattagupta, A.

Frydman, S. Sengupta, and P. A. Sreeram, **Virtual Journal of Nanoscale Science and Technology, February 14, 2005**

Contents

1 Introduction **1**

2 Fundamentals: **6**

2.1 Domain Assumption 6

2.2 Origin of Domains 8

2.3 Transition Region Between Domains 10

2.4 Single domain particle 12

2.5 Effect of temperature on single domain nanomagnets 15

3 Basic principles of measurement and instrumentations **20**

3.1 Introduction 20

3.2 X-Ray Diffraction 20

3.2.1 Scherrer Formula 20

3.2.2 Instrumental Line Broadening 23

3.3 Transmission Electron Microscope (TEM) 24

3.4 Superconducting Quantum Interference Device 25

3.5 Mössbauer spectroscopy 28

3.5.1 Mössbauer Spectra in a Fluctuating Magnetic Field 31

4 The effect of a weak ferromagnetic matrix on a system of nanomagnetic particles **42**

5 Tuning the relaxation dynamics of nano-magnets via magnetization **55**

6 Magnetic coding in systems of nanomagnetic particles **68**

List of Figures

2.1 The origin of domains 10

2.2 The Bloch wall. 11

2.3 Types of simple domain arrangement in a small sphere with low anisotropy. 13

2.4 Decomposition of sphere into circular shells. 13

2.5 Decomposition of sphere into circular shells. 17

3.1 Elastic scattering of an incident E.M. wave by a charge distribution. 21

3.2 Schematic figure of a two-dimensional gratting 22

3.3 Schematic diagram of a Transmission Electron Micrograph instrument . . . 26

3.4 Schematic diagram of Fe^{57} nuclear energy levels (a) Unsplitted and unshifted energy levels of Fe^{57} nucleus (b) Isomer shift(δ)(c) Zeeman splitting (c) Quadrupole splitting(ΔE) 29

4.1 Transmission electron micrographs of (a) Ni nanoparticles embedded in graphitic carbon, and (b) Ni particles coated by gold nanocrystals. The left panels are conventional low magnification TEM images and the right panels are high resolution TEM images taken at different sections of the samples. 45

4.2 FC and ZFC M(T) plots for Ni-C (top) and Ni-Au (bottom) nanoparticle systems. 46

4.3 Room temperature hysteresis loops for the Ni-C (top) and the Ni-Au (bottom) samples 47

4.4 Relaxation response graphs for Ni-C (top) and Ni-Au (bottom) nanoparticle systems. 49

5.1 X-Ray diffraction pattern of two samples (a)Sample 1 (b) Sample 2 57

5.2 High resolution transmission electron micrograph of Sample 1, to study the morphology and to estimate the 'd' value of the crystal planes 58

5.3 Field-Cooled (upper) and Zero Field-Cooled (lower) magnetization curves of (a)Sample 1 and (b)Sample 2 with H=100Oe 59

5.4 figure (a) (Top panel)saturation magnetization of Sample 1 and 2 as function of temperature, figure (b) is corecivity of Sample 1 and 2 as function of temperature. Inset is the simulated DC M-H measurement of Sample 1 and Sample 2. It can be seen that small particle (o) with large saturation magnetization can have larger coercivity than the large particle (+) with small saturation magnetization for same characteristic time scale of measurement. 60

5.5 Fitted Mössbauer spectra of two samples taken at room temperature and at 21K, using mossbauer line shape equation with a bimodal distribution of particle size. (a)Sample 1 at room temperature (b)Sample 2 at room temperature (c)Sample 1 at 21K and (d)Sample 2 at 21K 61

6.1 micrographs of $Ni_{0.35}Zn_{0.65}Fe_2O_4$ particles with diameters ranging from 10 to 100 nm.. 75

6.2 M(T) curves while cooling (open circle) and heating (solid circle) of the nanomagnetic particle systems at 50Oe. During the cooling process the following magnetic fields changes were performed: At 40K a 400Oe is applied and at 24K the field is switched off (top panel), at 50K the field is switched off and at 30K a 400Oe field is applied (middle panel), a 400Oe field is applied both at 50K and at 30K (bottom panel). Note that the heating curves show different "wiggles" for the increase or decrease of magnetic field during the cooling process. 76

6.3 M(T) curves for the cooling (open circle) and heating cycle (solid circle) while switching off the field at 40K and applying a *800Oe* field at 24 K. In this case, the signature of the field switching off at 40K is erased from the heating curve. 77

6.4 Results of our simulations for a system in which the sample was cooled (open circle) at a magnetic field, H. At T=60K the field is switched off and the temperature of the system is arrested before restore the field H and at 20K a field of 2H (top panel) or 5H (bottom panel) is applied. Note that the application of a large field erases the effect of the previous magnetic field switching off. The solid circles in the figure are the magnetization during heating cycle. 78

Chapter 1

Introduction

The unusual properties exhibited by nano-size materials have generated great interest among researchers, because of the posibility of promising applications in fields as divese as magnetic recording, ferrofluids, catalysts, colour imaging and pigments in paints, ceramics etc [1, 2]. The basic goal of this research is to understand how bulk properties change as one or more of the dimensions of a sample are reduced to scales a few order of magnitudes of atomic sizes [3, 4]. Magnetic properties are ones that are most affected by the change in size and do indeed present several new features [5]. Finite size effects dominate the magnetic properties of nanosized magnetic materials and become more important as the particle size decreases, because of the competition between surface and core magnetic properties.

One of the most interesting properties exhibited by ultrafine magnetic material is superparamagnetism [6, 7]. It is well known that below a critical particle size it is energetically preferable to have a single domain magnetic particle [8], where all the atomic spins are parallel to each other and this particle shows a giant magnetic moment. Magnetic anisotropy energy keeps such a particle magnetized in a particular direction and is generally proportional to the volume of the particle.

At finite temperatures a sample which is small enough to comprise of a single domain exhibits "Superparamagnetic" behaviour i.e. fluctuation of magnetization between the easy directions occurs at a rate faster than the characteristic time scale of the measuring instruments. The magnetism of such a single domain particle has been an active field of research since the pioneering work of Stoner and Wolfarth [9], Neel [10] and Brown [11]. Superparamagnetic behaviour has currently been studied by a number of experimental

techniques such as ac and dc susceptibility measurements[12, 13, 14, 15] , neutron diffraction [16] , Mössbauer spectroscopy [17], transverse susceptibility [18] etc..

Further, the subject of how a bulk magnetic specimen acquires a single domain structure and exhibits magnetic viscosity due to Neel relaxation, when its size is reduced, is a problem what has been studied for quite some time [19, 20, 21]. We have already mentioned that when the relaxation time τ is smaller than the measurement time, the specimen shows superparamagnetic behaviour whereas in the opposite limit, relaxation is arrested. The crossover mark, derived from the temperature dependence of τ, yields the concept of 'blocking temperature' (T_B). When $T<T_B$, one has a frozen moment, whereas for $T>T_B$, one sees magnetic viscosity. Thus single-domain magnetic particles have provided a happy hunting ground for studying nonequilibrium phenomena, characterized by irreversibility, hysteresis and other memory effects.

In recent times this subject has attracted a great deal of attention in view of the heightened interest in nanoscience and magnetic memory devices. As it turns out, it is not just the temperature T which can be used as a control parameter but even the mean size and inter-particle interaction can be profitably tuned because of the exponential dependence of τ on the volume (V) of the particle. This was demonstrated in our recent measurements and analysis of irreversible magnetization through cooling and heating cycles[22].

Recently enormous effort has been expended to produce samples of mono dispersed particles. But we shall show in the following chapters that polydispersed materials are also very useful in some situations. Polydispercity (i.e. size-distribution) can be tuned to yield important "Memory" effect which we shall discuss in the Chapter 6.

Thus one of the principle foci in this thesis will be the study of the effect of interparticle interaction and polydispersity in nanomagnetic systems.

The outline of the thesis as follows : In Chapter 2 we survey some basic properties of classical spin systems. In chapter 3 we have discussed the basic mesurement techniques we have used for our experimental purpose. Chapter 4 deals with effect of the background medium on the magnetic properties and relaxation dynamics of the nanomagnetic particles, on two samples namely Ni-coated by carbon and Ni-coated by gold. In Chapter 5 we report how the relaxation dynamics of nanomagnetic particles can be tuned via their magnetization, we have used two samples of $Ni_{0.65}Zn_{0.35}Fe_2O_4$ for this purpose. In

chapter 6 we show the possibility of storing binary numbers in a system of polydispersed nanomagnetic samples during a temperature cycle. We have used some new magnetic measurement protocols on $Ni_{0.65}Zn_{0.35}Fe_2O_4$ sample to store binary numbers ("0"/"1") in it.

Bibliography

[1] A. N. Goldstein *and Book of Nanophase Materials* (New York Marcel Dekker Inc.) (1997).

[2] J. L. Moran-Lopez and J. M. Sanchez *New Trends in Magnetism, Magnetic Materials and Their Applications* (New York : Plenum Press) (1994).

[3] K. M. Unruh and C. L. Chein in *Nanomaterials : Synthesis, Properties and Application*(ed.), A. S. Edelstein and R. C. Cammarata (Bristol : Institute of Physics)(1996).

[4] I. S. Jacobs and C. P. Bean in *Magnetism III* (eds.), G. T. Rado and H. Suhl (New York : Academic)(1963).

[5] G. C. Hadjipanayis, K. J. Klabunde and C. M. Sorensen in *Nanomaterials : Synthesis, Properties and Applications* (eds) A. S. Edelstein and R. C. Cammarata (Bristol : Institute of Physics)(1996).

[6] E.P.Wohlfarth, J.Phys.**F10**,L241(1980).

[7] R. Street and J. C. Woolley, Proc. Phys. Soc London, Sec A **62**, 562 1949. Also reviewed in S.Dattagupta, *Relaxation Phenomena in Condensed Matter Physics, Chapter XV*, Academic Press, Orlando(1987).

[8] C. Kittle, Rev. Mod. Phys. **21**, 541 (1949).

[9] E. C. Stoner and E. P. Wohlfart Philos. Trans. R. Soc. London Ser. A **240**, 599(1948).

[10] L. Neel, Ann. Geophys. **5**, 99(1949).

[11] W. F. Brown Jr, Phys. Rev. 130, 1677 (1963).

[12] J. L. Dormann, L. Bessais and D. Fiorani J. Phys. C **21**, 2015(1988).

[13] W. Lue *et al.*, Phys. Rev. Lett. **67**, 2721(1991).

[14] C. Johansson *et al.*, J. Magn. Magn. Mater. **122**, 125(1993).

[15] D. P. E. Dickson *et al.*, J. Magn. Magn. Mater. **125**, 325(1993).

[16] I. Mirebeau *et al.*, J. Magn. Magn. Mater. **104-107**, 1560 (1992).

[17] A large body of work on Mössbauer effect in single domain magnetic particles has been carried out by S. Mϕrup and his group. A recent reference is: M. F. Hansen, C. B. Koch, and S. Mϕrup, Phys. Rev. B **62**, 1124-1135 (2000).

[18] A good amount of work on transverse susceptibility has been carried out by S. Hariharan and his group.

[19] J. Frenkel and J. Dorfman, Nature (London) **126**, 274 (1930); C. Kittel, Phys. Rev. **70**, 965 (1946).

[20] C. P. Bean and J. D. Livingstone, J. Appl. Phys. **30**, 1205 (1959); I. S. Jacobs and C. P. Bean, in magnetism, vol. III, (G. T. Rado and H. Suhl, eds.) Academic Press, New York, 1963.

[21] L. Neel, Ann. Geophys. **5**, 99 (1949).

[22] S. Chakraverty, B. Ghosh, S. Kumar, A. Frydman Appl. Phys. Lett. 88, 042501 (2006).

Chapter 2

Fundamentals:

In this chapter we discuss a few fundamental concepts involving magnetic materials which we shall need in our subsequent work. Our discussion is organized according to the historical development of the subject wherein we first analyse how experimental observations of the M-H curve of a ferromagnetic material led Pierre Weiss (in 1907)[1] to propose the"domain idea". This section will be followed by the discussion on how different contributions such as exchange, anisotropy and magnetic energy compete with each other to give rise to domain structures in ferromagnetic materials, as pointed out by Landau and Lifshitz. We then discuss the transition layer between two domains, which is very crucial for the understanding of the possibility of obtaining a single domain magnetic particle with reduction of particle size, a primary concern of this thesis.

2.1 Domain Assumption

The main essence of ferromagnetism is illustrated by the fact:
It is possible to change the over-all magnetization of a suitably prepared ferromagnetic specimen from an initial value of zero (in absence of an applied magnetic field) to a saturation value of order of 1000 gauss, by the application of a field whose strength may be of the order of 0.01 Oersted (Oe). - Charles Kittel[2]
The above mentioned observation contains two significant suggestions.
(1) It is possible in some cases to attain saturation magnetization by the application of a very weak magnetic field.
(2)It is possible for magnetization of the same specimen to be zero in nearly zero field.

The first observation is remarkable since it is known from the study of paramagnetism that the application of a field of 0.01 Oersted has an entirely negligible effect on the magnetization of a system of free and independent elementary magnetic moments. For example, at room temperature a field of 0.01Oe will increase the magnetization of paramagnetic salt by about 10^{-6} gauss, as compared with 10^3 gauss in a ferromagnetic specimen. The small effect in case of the paramagnet is known to be caused by thermal agitation which acts in such a manner as to oppose the ordering influence of the applied magnetic field.

Pierre Weiss (1907) [1] pointed out that the randomization caused by thermal agitation could be largely circumvented if one postulated in ferromagnetic materials the existence of a powerful internal "molecular" field; the mutual interaction between the electrons which tend to line up the magnetic moments parallel to one another.

The required magnitude for the Weiss molecular field may be estimated readily. At the Curie temperature T_c the thermal energy $k_B\mathrm{T}_c$ of an electron spin is of the same order of magnitude as the interaction energy $\mu_B\mathrm{H}_{mf}$ of the magnetic moment μ_B of an electron acted on by the effective molecular field H_{mf}:

$$k_B T_c \sim \mu_B H_{mf}, \tag{2.1}$$

so that,

$$H_{mf} \sim k_B T_c/\mu_B \sim 10^{-16}10^3/10^{-20} \sim 10^7 Oe. \tag{2.2}$$

This is an extremely powerful effective field; it is about twenty times more intense than any actual magnetic field produced in a laboratory. At temperatures below T_c the effect of molecular field outweighs the thermal fluctuation energy and the specimen is accordingly ferromagnetic. This explains the first point.

The second observation had been explained by Weiss in the following way: Weiss made the assumption that actual specimens are composed of a number of small regions called domains, within each of which the local magnetization is saturated; the directions of magnetization of different domains need not be parallel. However, the increase in the value of the resultant magnetic moment of the specimen under the action of an applied magnetic field may be imagined to take place in the domain theory by two independent

processes, as was suggested by R. Becker[3, 4]: by an increase in the volume of domains, which are favorably oriented with respect to the field at the expense of unfavorably oriented domain; or by rotation of the directions of magnetization towards the direction of the field.

It turns out on the closer examination that in weak fields the magnetization changes usually proceed by means of domain boundary displacements, so that the domains change in size. In strong fields the magnetization usually changes by means of rotation of the direction of magnetization.

We, therefore, see that Weiss was able to explain the principal aspects of ferro-magnetism by means of two assumptions: the existence of a molecular field and the existence of domain structure. Weiss did not justify either of these assumptions in term of atomic forces.

Let us now qualitatively discuss the causes responsible for the formation of domain.

2.2 Origin of Domains

Landau and Lifshitz[5] showed that domain structure is a natural consequence of competition between various contributions namely exchange, anisotropy, and magnetic energy of a ferromagnetic body.

Before going into the details of the explanation, let us recall the three relevant energies[6, 7, 8] in brief.

1. Exchange : This is electrostatic energy beween two electrons follewed by Pauli exclusion principle. The exchange energy between two electrons with spin S_1 and S_2 is given by,

$$E_{ex} = -2JS_1 \cdot S_2, \tag{2.3}$$

where J is known as exchange integral. The exchange integral J is grater that zero for ferromagnetic materials and J is less than zero for antiferromagnetic materials.

2: Anisotropy : The term anisotropy is used to describe the dependence of the internal energy on the direction of spontaneous magnetization. We call an energy term of this kind a magnetic anisotropy term. Generally the magnetic anisotropy term has

the same symmetry as the crystal structure of the material, and we may describe it as magnetocrystalline anisotropy. The simplest case is a uniaxial magnetic anisotropy. For example, hexagonal cobalt belongs to this group, where spins find their anisotropy minima along the C-axis of the crystal structure. Throughout this thesis we shall restrict ourselves to this kind of simple uniaxial anisotropic case, where the anisotropy energy is given by,

$$E_a = K_1 \sin^2 \theta, \tag{2.4}$$

where K_1 the anisotropy constant, has typical value $\sim 10^6$ erg cm^{-3} and θ is the angle between the spin and easy axis.

3. Magnetostatic energy : In saturated magnetic specimen of finite size, the effective free poles which appear on its surface will produce a magnetic field directed opposite to the magnetization. This field is called demagnetization field. The intensity of the demagnetizing field H_d is proportional to effective free pole density and, therefore, to the existing magnetization itself, namely

$$H_d = NI, \tag{2.5}$$

where I is the magnetization and N is called the demagnetization factor, which depends only on the shape of the specimen, for example $N = 1/3$ for a spherical sample.
We may understand the origin of domain by considering the structures shown in the Fig. 2.1, each representing a cross section through a ferromagnetic single crystal.
In (a) we have a single domain; as a consequence of the magnetic "poles" formed on the surface of the crystal this configuration will have a high value of magnetic energy $(1/8\pi)\int B^2$ dV. The magnetic energy density for the configuration shown will be of the order of ${M_s}^2 \sim 10^6$ erg/cc; here M_s denotes the saturation magnetization, where we use cgs units.
In (b) the magnetic energy is reduced by roughly one-half by dividing the crystal into two domains magnetized in opposite direction.
In (c) with N domains the magnetic energy is reduced to approximately $1/N$ of the magnetic energy of (a), because of the reduced spatial extension of the field.
In domain arrangements such as (d) and (e) the magnetic energy is zero. Here the boundaries of the triangular prism domains near the end of the faces of the crystal make equal

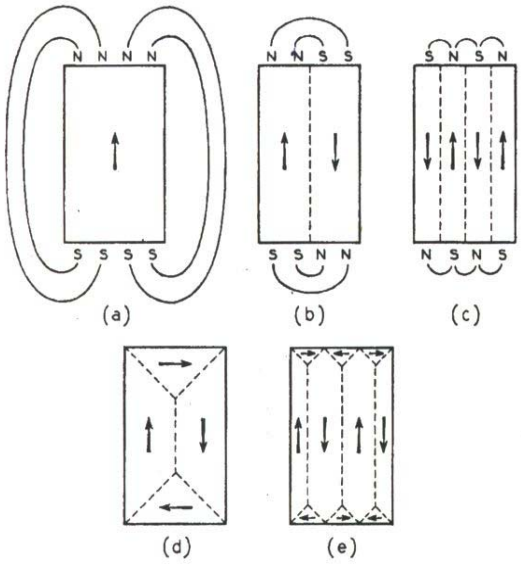

Figure 2.1: The origin of domains

angles (45^0) with the magnetization in the rectangular domains and with the magnetization with the domain of closure. The component of the magnetization normal to the boundary is continuous across the boundary and there is no magnetic field associated with the magnetization. The flux circuit is completed within the crystal-thus giving rise to the term **domain of closure** for surface domains that complete the flux circuit.
Domain structures always have their origin in the possibility of lowering the energy of the system by going from a saturated configuration with high magnetic energy to a domain configuration with a lower energy - Kittel.

2.3 Transition Region Between Domains

A **Bloch wall** in a crystal is the transition layer that separates adjacent regions (domains) magnetized in different directions. The entire change in spin direction between domains does not occur in one discontinuous jump across a single atomic plane, but takes place in a gradual way over many atomic planes (Fig. 2.2). The exchange energy is lower when the change is distributed over many spins.
This behavior may be understood by interpreting the Heisenberg equation classically. We

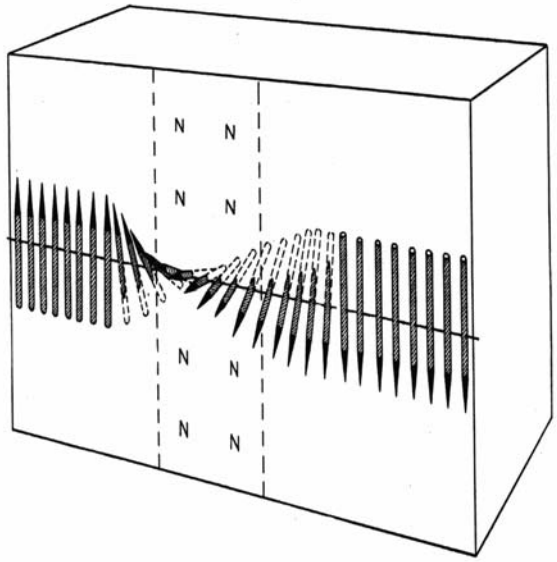

Figure 2.2: The Bloch wall.

replace $\cos\phi$ by $(1\text{-}\frac{1}{2}\phi^2)$, for small enough ϕ; then $w_{ex} = JS^2\phi^2$ is the exchange energy between two spins making an angle ϕ with each other. Here J is the exchange integral and S is the spin quantum number; w_{ex} is referred to the energy for parallel spins.
If a total change of π occurs in N equal steps, the angle between neighboring spins is π/N, and the exchange energy per pair of neighboring atoms is $w_{ex} = JS^2((\pi/N)^2)$. The total exchange energy of a line of $N+1$ atoms is,

$$Nw_{ex} = JS^2(\pi^2/N). \tag{2.6}$$

The wall would thicken without limit were it not for the anisotropy energy, which acts to limit the transition layer. The spins contained within the wall are largely directed away from the axis of easy magnetization, so there is an anisotropy energy associated with the wall, roughly proportional to the wall thickness.
Consider a wall parallel to the face of the simple cubic lattice and separating domains magnetized in opposite direction. We wish to determine the number N of atomic planes contained within the wall. The energy per unit area of the wall is sum of the contributions from exchange and anisotropy energies: $\sigma_W = \sigma_{ex} + \sigma_{anis}$.

The exchange energy is given approximately by Eqn. 2.6 for each line of atoms normal to the plane of the wall. There are $1/a^2$ such lines per unit area, where a is the lattice constant. Thus $\sigma_{ex} = \pi^2\ JS^2/Na^2$.
The anisotropy energy is of the order of the anisotropy constant times the thickness Na, or $\sigma_{anis} \sim KNa$; therefore,

$$\sigma_W \sim (\pi^2 JS^2/Na^2) + KNa. \tag{2.7}$$

This is a minimum with respect to N when

$$\delta\sigma_W/\delta N = 0 = -(\pi^2 JS^2/N^2a^2) + Ka; \tag{2.8}$$

or

$$N = (\pi^2 JS^2/Ka^3)^{1/2}. \tag{2.9}$$

The total wall energy per unit area on this model is

$$\sigma_W = 2\pi(KJS^2/a)^{1/2}; \tag{2.10}$$

2.4 Single domain particle

Starting from bulk it is always possible to achieve a critical particle size below which there is transformation from multi-domain to single domain structure. In the following section we are going to estimate that critical particle size from energy considerations.
Let us consider a small spherical particle of radius R; it is supposed for the sake of concreteness that the particle is a single crystal. We are interested first of all in critical particle size for which the energy of the single domain configuration is lower than the energy of configurations in which there is a domain structure tending towards flux closure.

The energy of the saturated single domain configuration is in the form of magnetostatic energy, and is equal to,

$$f = \frac{1}{2} N {I_s}^2 = 2\pi {I_s}^2/3 \tag{2.11}$$

Figure 2.3: Types of simple domain arrangement in a small sphere with low anisotropy.

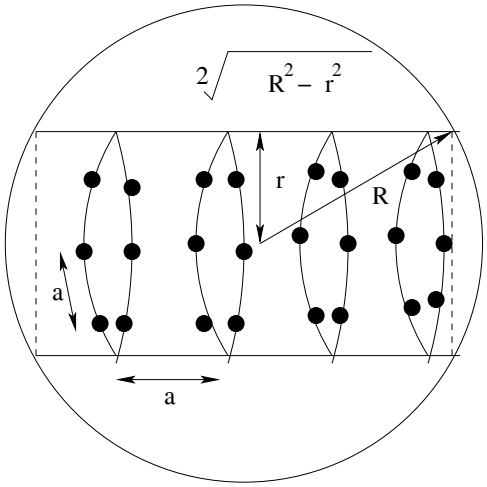

Figure 2.4: Decomposition of sphere into circular shells.

for a sphere; where N is the demagnetization factor and I_s is the saturation magnetization of the system. The numerical value is approximately 6×10^6 erg/cc in case of iron. For a sphere of radius R the total energy is

$$w = fV = (1/2)(4\pi/3)^2 R^3 {I_s}^2 \tag{2.12}$$

and is approximately equal to 24×10^6 ergs for $R = 1$ cm and 24×10^{-12} ergs for $R =10^{-6}$ cm.

As an example of the estimation of the critical radius let us consider a magnetic particle with low anisotropy. In this case it appears reasonable to take the circular configuration shown in the Fig. 2.4 as most favorable flux-closure configuration. The energy here is largely in the form of exchange energy. Consider the spins on a circular ring of radius r. There are $2\pi r/a$ spins on the ring, where a is the lattice constant. The total change in angle in going around once is 2π, so that the angle ϕ between successive spins is ϕ=a/r and the exchange energy is

$$w_{ring} = (1/2)J(a/r)^2(2\pi r/a) = \pi Ja/r, \tag{2.13}$$

taking the spins of the system S =1. Now consider the sphere made up of circular cylinders (Fig. 2.4), each one unit in thickness. The number of rings (separated by the lattice dimension a) in a cylinder is $(2/a)(R^2 - r^2)^{1/2}$, so that,

$$w_{cyl} = 2\pi J(R^2 - r^2)^{1/2}/r, \tag{2.14}$$

$$\begin{aligned} w_{sphere} &= (2\pi J/a)\int_a^R [(R^2 - r^2)^{1/2}/r]dr \\ &\sim (2\pi JR/a)[ln(2R/a) - 1], \end{aligned} \tag{2.15}$$

or per unit volume,

$$f_{ex} = (3/2)(J/aR^2)[ln(2R/a) - 1]. \tag{2.16}$$

This energy density depends on the size of the sphere. Taking $J/a = 2\times10^{-6}$ ergs/cm for iron we have for

(a) R=1 cm ; w_{ex}=1.3×10^{-4}ergs

(b) R=10^{-6} cm ; w_{ex}= 23×10^{-12}ergs
and
f_{ex}= 0.8×10^{7} ergs/cc.
It is seen that the flux-closure configuration has by far the lower energy when the radius is 1 cm, but when the radius is 10^{-6} cm the saturated configuration has lower energy. Thus for sufficiently small particles saturated configuration has a lower energy than the flux-closure configuration. The critical radius R_c is given by,

$$(1/2)(4\pi/3)^2 {R_c}^3 {I_s}^2 = (\pi J R_c/a)[ln(2R_c/a) - 1]. \tag{2.17}$$

and is approximately inversely proportional to the saturation magnetization. The value of critical radius for iron ∼10^{-6} cm[9, 10].

2.5 Effect of temperature on single domain nanomagnets

So far we have discussed how different magnetic energies compete with each other to give rise to domain structure in a bulk ferro magneti material, we have also discussed the possibility of single domain magnetic structure below a critical particle volume.
We now turn attention to the main focus of the present chapter, namely a ferromagnetic material below that certain critical size(typically ∼ 15nm in radius) consists of a single magnetic domain in which a large number of magnetic moments (∼ 10^5 in number) get coherently locked up in unison. This phenomenon was frist recognized by Frenttel and Dorfman [11]. Single domain nanoparticle have a remarkable range of applications, from magnetic recording media to catalysis, ferrofluids, magnetic imaging and refrigeration, not to mention paleomagnetism. A study of relaxation effects in nanomagnetic particles is particularly important for storage media and memory devices, this also clarifies our understanding of similar phenomena in molecular magnetic clusters, nematic liquid crystals, relaxor ferroelectric and micromagnetic-like spin glasses.
Most of the observed effects in the single-domain magnetic particles are due to magnetic anisotropy, the energy for which depends on the orientation of the magnetization vector of the domain relative to the crystalline axes.
We shall restrict our further discussion to the simplest form of anisotropy which is a

uniaxial one (applicable to single-domain particle of Co, say), and given by [12]

$$E(\theta) = KV\sin^2\theta, \tag{2.18}$$

where K is the so called anisotropy energy per unit volume, V is the volume of the particle and θ is the angle between the magnetization vector and the crystalline anisotropy axis. If a field H is applied along the easy axis (E.A.) the energy becomes

$$E(\theta) = KV\sin^2\theta - \mu VH\cos\theta, \tag{2.19}$$

where μ is the magnetic moment per unit volume. The equilibrium value of magnetization is then given by

$$M_{eq} = V\mu\langle\cos\theta\rangle_{eq}, \tag{2.20}$$

where

$$\langle\cos\theta\rangle_{eq} = \frac{\int_0^\pi d\theta\sin\theta\cos\theta e^{-\frac{E(\theta)}{k_BT}}}{\int_0^\pi d\theta\sin\theta e^{-\frac{E(\theta)}{k_BT}}} \tag{2.21}$$

For very weak anisotropy (K $\sim$ 0), eq.2.21 reduces to the usual Langevin function for classical paramagnets :

$$\langle\cos\theta\rangle_{eq} \sim \coth\left(\frac{\mu VH}{k_BT}\right) - \frac{k_BT}{\mu VH}. \tag{2.22}$$

On the other hand, if the anisotropy is very large (KV $\gg$ μ V H), the magnetic moment is "locked" at the orientation of 0 or π, and hence we may use the 'two-state' limiting formula for :

$$e^{\frac{KV\sin^2\theta}{k_BT}} \sim \frac{1}{2}[\delta(\cos\theta - 1) + \delta(\cos\theta + 1)] \tag{2.23}$$

In that case

$$\begin{aligned}\langle\cos\theta\rangle_{eq} &= \frac{\int_0^\pi d\theta\sin\theta\cos\theta[\delta(\cos\theta-1)+\delta(\cos\theta+1)]e^{\frac{\mu HV\cos\theta}{k_BT}}}{\int_0^\pi d\theta\sin\theta[\delta(\cos\theta-1)+\delta(\cos\theta+1)]e^{\frac{\mu HV\cos\theta}{k_BT}}} \\ &= \tanh\left(\frac{\mu VH}{k_BT}\right).\end{aligned} \tag{2.24}$$

In either of this two limits, the average magnetization is independent of anisotropy parameter K (eqs. (2.22) and (2.24)).

Until now we have discussed the magnetization properties of single-domain particles when

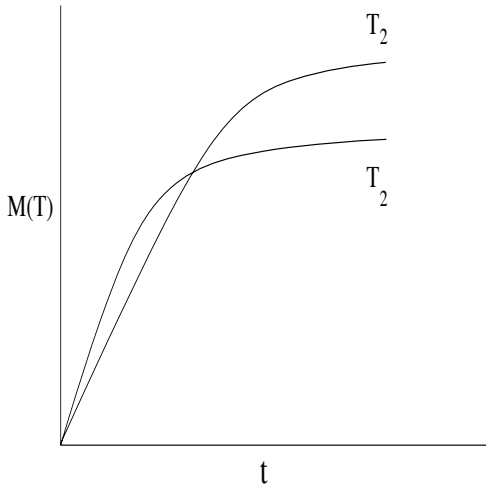

Figure 2.5: Decomposition of sphere into circular shells.

they are in thermal equlibrium. Let us now consider the conditions under which an assembly of (non-interacting) single-domain particles may reach thermal equlibrium in a time short compared with the time of an experiment. In a solid, Neel [13] showed that for a small enough particle, the total magnetization as a whole, composed of large number of moments coherently locked-in unision, can undergo rotational relaxation over the anisotropy energy barrier, given by eq.2.19. The corresponding Neel relaxation time (for H = 0) is given by

$$\tau = \tau_0 exp(KV/k_BT), \tag{2.25}$$

where the pre-factor τ_0 before the exponential is typically of the order of 10^{-9} to 10^{-10} sec. The dependence of exponent on the volume V of the particle makes τ an extremely sensitive function of particle-size indeed. For instance, for a spherical iron particle where only source of anisotropy is its first order crystal anisotropy, a particle 11.5 nm in radius will have a τ of the order of 10^{-1}sec at room temperature. Such a particle would then reach equlibrium quite rapidly. But a slightly bigger particle of radius 15nm will take enormously long time of 10^9sec to relax and therefore, wiil be highly stable.

The above discussion bring us then to the issue of 'time-window' effect in the relaxation behaviour of single-domain nano magnetic particles. If $\tau > \tau_{exp}$, where τ_{exp} is a typical experimental time-window (to be elaborated later) the magnetization vector will appear effectively 'frozen'. On the other hand, for $\tau < \tau_{exp}$, the magnetization will sample both

θ=0 and $\theta = \pi$ configurations equally and a few times, thereby yielding a paramagnetic response. Because one is dealing here with not an ordinary paramagnet but a 'giant' moment comprising nearly 10^5 in a 'locked-in' orientation, the underlying phenomenon is reffered to as "Super paramagnetic relaxation". In the regim of $\tau_{exp} < \tau$ the assembly of magnetic nanoparticle will exhibit what is called "magnetic viscosity" and therefore, marked hysteresis effect. The crossover point given by $\tau = \tau_{exp}$ leads to an important concept in the field, viz., that of the "Blocking Temperature" T_B. When T<T_B, the moments are frozen, whereas when T>T_B, one see time-dependent 'viscous' effect.

While the above analysis is valid for zero magnetic field, the application of an external magnetic field allows for a further tuning of relaxation time. For weak magnetic field (compared to the anisotropy energy) the relaxation times are approximated by

$$\tau_{\pm} = \tau_0 exp\left(\frac{KV \pm \mu VH}{k_B T}\right), \tag{2.26}$$

where + corresponds to relaxation out of the θ=0 orientation whereas - corresponds to relaxation out of the $\theta = \pi$ orientation.

What is also interesting to note is that it is not only the equlibrium value of the magnetization but the relaxation time too that depends on all the three parameters, H, T and V, that can be tuned in the laboratory. For instance, if one considered two M(t) vs t curves at two different temperatures T_1 and T_2 ($T_2 > T_1$), all other parameters remaining the same, one would qualititavely arrive at a diagram given by fig.2.5:

Now, although the asymptotic response for larger temperature T_2 is smaller, response is faster, in accordance with the Neel/Arrhenius expression of eq. 2.26. Therefore, if one were to make a 'nonequlibrium measurement', one may find the magnetization value to be even larger at higher temperature - a clear counterintutive issue but one of great significance in dealing with memory effects,and can be used to understand memory effect described in chapter 6.

Bibliography

[1] P. Weiss, J. de Phys. et rad. 8, 358 - 690 (1907).

[2] C. Kittel, Rev. of Mod. Phys. 21, 541 (1949).

[3] R. Becker, Zeits. f. Physik, 62, 253 - 269 (1930).

[4] R. Becker, Physik. Zeits, 33, 905 - 913 (1932).

[5] L. Landau and E. Litshtz Physik. Zeits. Sowjetuion, 8, 153 - 169 (1935).

[6] C. Kittel, Introduction to Solid State Physics (John Wiley & Sons, USA).

[7] Soshin Chikazumi, Physics of Ferromagnetism (Oxford university press, UK, 1997).

[8] A. H. Morrish, The Physical Principles of Magnetism (John wiley & Sons, USA).

[9] C. Kittel, Phys. Rev. 70, 965 - 971 (1948).

[10] L. Neel, Compets rendus (Paris) 224, 1488 - 1490.

[11] J.Frenttel and J.Dorfman, Nature 126, 274 (1930).

[12] C.P. Bean and J.D. Livingstone, J.Appl. Physics 30, 1205,1959.

[13] Neel, Compt. rend. underline228, 664, 1949; Ann. geophys. J, 99, 1949.

Chapter 3

Basic principles of measurement and instrumentations

3.1 Introduction

In this Chapter we discuss the measurement tools used in our experiments and outline the basic principles involved. In the first section we shall discuss the X-Ray diffraction technique and how the broadening of an X-Ray peak can be used to estimate the average particle size of a system of nanoparticles. This will be followed by a discussion on how the width of an X-ray diffraction peak is modified due to instrumental broadening. We then present the basic principle of Transmission Electron Microscopy. In the third section we shall outline the operating mechanism of a SQUID magnetometer. In the last section we explain the basics of Mössbauer spectroscopy, which can be used as a powerful local probe.

3.2 X-Ray Diffraction

X-Ray diffraction is one of the most powerful and commonly used techniques to identify the phase of a sample. This method is also useful to analyse the crystallographic properties of the sample in great detail. Some basic aspects of the X-ray diffraction method is set forth below.

3.2.1 Scherrer Formula

Let us consider an electromagnetic wave of wave vector $\vec{K}_i$ incident on a charge distribution ($\rho(\vec{r})$). Let us also assume that this incident wave suffers an elastic collision from a

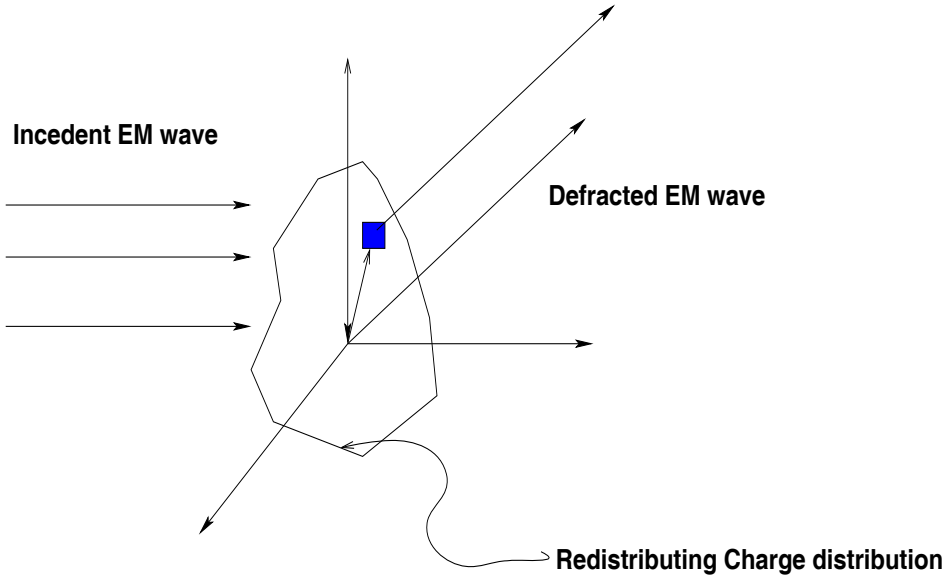

Figure 3.1: Elastic scattering of an incident E.M. wave by a charge distribution.

distributing charge of density $\rho(\vec{r})$. The path difference between the a ray scattered from the origin and a ray scattered by any other volume element (say at $\vec{r}$) toward at particular direction is $(\hat{K}_f.\vec{r} - \hat{K}_i.\vec{r})$ (fig.3.1) (where $\hat{K}_f$ and $\hat{K}_i$ are the unit vector along the wave vector of the scattered and incident ray respectively) and hence the corresponding phase difference is $\frac{2\pi}{\lambda}[(\hat{K}_f - \vec{K}_i).\vec{r}]$. Let us write $(\vec{K}_f - \vec{K}_i) = \vec{q}$. The amplitude of scattering due to the elemental volume $d^3\vec{r}$ is proportional to the amount of the charge in the scattering element. Hence the scattering amplitude from the entire charge distribution is given by

$$\int e^{i\vec{q}.\vec{r}}\rho(r)d^3\vec{r}. \tag{3.1}$$

Hence the amplitude of scattered ray is nothing but the Fourier transform of the charge distribution.

Let us consider a one dimensional grating (fig.3.2) with N rulings, with inter-ruling separation, d. Hence the length of the grating is t=Nd. The $\rho(\vec{r})$in this case is $\rho(x) = \sum_{n=0}^{N}\delta(x - nd)$ and hence the scattering amplitude is given by

$$A \sim \int e^{iKxsin\theta}\sum_{n=0}^{N}\delta(x - nd)dx = \sum_{n=0}^{N}e^{iknd\sin\theta}. \tag{3.2}$$

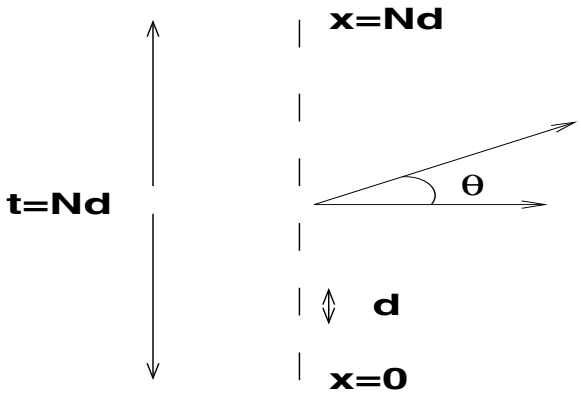

Figure 3.2: Schematic figure of a two-dimensional gratting

The intensity of diffracted ray [I $\sim \|A\|^2$] is thus given by

$$I(\theta) = I_0 \frac{sin^2(\frac{KNd}{2}sin\theta)}{sin^2(\frac{Kd}{2}sin\theta)}. \tag{3.3}$$

The above expression implies that the diffraction peak will be appeared at

$$\frac{Kd}{2}sin\theta = m\pi : m = 0, 1, 2.... \tag{3.4}$$

which leads us to famous diffraction law [1]

$$2dsin\theta = m\lambda. \tag{3.5}$$

From the above analysis it is clear that for an infinite grating, the delta function peak will appear in the diffraction pattern. But the finite size of the grating will produce a broadening in the peak of the diffracted ray. This broadening (δ) is given by

$$\delta = \frac{2\pi}{Ktcos\theta}. \tag{3.6}$$

which gives the length of the finite grating

$$t = 0.9\frac{\lambda}{\delta cos\theta} \tag{3.7}$$

The above formula is readily generalized to a three dimensional periodic crystal of finite size and is known as the famous Sherrer equation [2]. We shall use this equation to find out the average diameter of the nanoparticles.

We have carried out X-Ray diffraction measurements on our sample to identify the phase of our sample. The mean particle diameter of the nano-particle and average lattice parameter of the ferrite particle was also determined from XRD. We have used an $X-$ray diffractometer (Philips, PW 1710) with CuK_α radiation ($\lambda = 1.5409\mathring{A}$) for the above mentioned purpose.

3.2.2 Instrumental Line Broadening

X-Ray diffractometer may have some intrinsic line width. This can produce error in the calculated particle size.

Let us consider the instrument having an intrinsic Gaussian line width, given by

$$P(y,x) = \frac{1}{\sqrt{\pi\sigma_I}} e^{-(y-x)^2/{\sigma_I}^2}, \tag{3.8}$$

instead of the ideal delta function $\delta(y-x)$ around x. The actual diffraction coming from the sample being

$$g_1 = \frac{1}{\sqrt{\pi\sigma_1}} e^{-(x-x_0)^2/{\sigma_1}^2}. \tag{3.9}$$

Hence the observed spectra will be a folding or convolution of g and P to give

$$\langle g(y)\rangle = \int g(x)P(y,x)dx. \tag{3.10}$$

which after integration and a little bit of algebra gives us

$$\langle g(y)\rangle = \sqrt{\frac{\sigma_1\sigma_I}{\pi({\sigma_1}^2+{\sigma_I}^2)}} e^{-(y-x_0)^2/({\sigma_1}^2+{\sigma_I}^2)} \tag{3.11}$$

It is clear from the above expression that the observed diffracted pattern is again Gaussian with peak at x_0 and the width is now modified to $({\sigma_1}^2+{\sigma_I}^2)$ and hence the δ of eqn.3.6 should be replaced by $\sqrt{\delta^2-{\sigma_I}^2}$, where index I and 1 corresponds to instrument and system respectively.

A similar analysis shows that for a Lorentzian instrumental line width will produce a observed line width of $\delta_1+\delta_I$. And hence the δ occuring in eqn.3.6 should be changed accordingly.

3.3 Transmission Electron Microscope (TEM)

The electron microscope has extended the resolution available for morphological studies from that dictated by the wavelength of visible length to dimensions which are well into the range required to image the lattice planes in any crystal structure.

The early development in electron microscopy was an international success story. In the immediate post-war period, the commercial transmission instrument were manufactured in Germany, Holland, Japan, the United Kingdom and the United States.
The transmission electron microscope [3] is in many ways analogous to a transmission optical microscope, usually 'upside down', in the sense that the source of the beam is at the top of the microscope 'column' while the recording system is at the bottom. The electron gun replaces the light source and is maintained at high voltage (typically 100-400Kev). A heated tungsten filament is capable of generating electron beam current density of the order 5×10^4 Am^{-2}, while lanthanum hexaboride crystals generate 1×10^{-6} Am^{-2}. The high energy electron gun is focused by an electromagnetic condenser lens system, whose focus is adjusted by adjusting the lens current(not lens position, as would be the case in the optical microscope). The specimen stage is much more complicated than indicated schematically in the diagram (fig.3.3) and allows for specimen to tilt as well as permitting a z-adjustment along the optic axis. An important point to note is that fine focusing of the image in the transmission electron microscope is not achieved by adjusting the position of the specimen along z-axis; rather by adjusting the object lens current. The final imaging system also employs electromagnetic lenses, and the final image is observed on a fluorescent screen. Typical screen current is in the range 10^{-10} to 10^{-11} Am^{-2}, but may even be lower at the highest magnification. Photographic emulsions are commonly used to record the final image.
The high energy electron has a very limited path length in air, so that the whole electron microscope column must be under vacuum. Specimen contamination under the beam is also a serious problem which may restrict viewing time for a particular area and limit the achievable resolution. In general, the vacuum should be better than 10 Torr, while for highest resolution a vacuum of 10^{-6} Torr is desirable and all sources of contamination

should then be trapped, usually by cryogenic cooling of the specimen surrounding.

The TEM micrograph of all the samples namely $Ni_{0.35}Zn_{0.65}Fe_2O_4$, Ni-C and Ni-Au have been taken. TEM micrograph indicates that the particle size follows a lognormal distribution. This distribution is given by :

$$f(y) = \frac{1}{ys\sqrt{2\pi}} e^{-(ln\frac{y}{y_0})^2/2s^2}, \tag{3.12}$$

where y is the particle diameter, y_0 is the most probable diameter and s controls the width of the distribution. Crystallographic detail as well as the interparticle separations of the samples were also estimated from TEM.

3.4 Superconducting Quantum Interference Device

We have used a Quantum Design MPMS-5S with a field range of -5T<H<5T and temperature range of 1.7K<T<400K. The heart of this machin is a Superconducting Quantum Interference Device (SQUID). We have used this device to make the DC M-H, FC-ZFC (field cooled and zero field cooled) magnetic measurements. We have studied the relaxation-response mechanism of our magnetic system and performed our binary number coding protocols on our magnetic nanoparticle sample employing the same instrument. A measurement is performed in SQUID by moving a sample through the superconducting detection coil, which is located at the centre of the magnet. As the sample moves along the detection coils the magnetic dipole moment of the sample induces an electric current through the detection coils. The SQUID functions as a highly linear current-to-voltage converter, so that variation in the current induced in the detection coils, produces corresponding variations in the SQUID output voltage.

The detection coils system is wound from a single piece of superconducting wire in the form of three counter-wound coils configured as a second-order gradiometer. In this geometry, the upper coil is composed of a single turn wound clockwise, the center coil comprises of two turns wound counterclockwise and the bottom coil is again a single turn

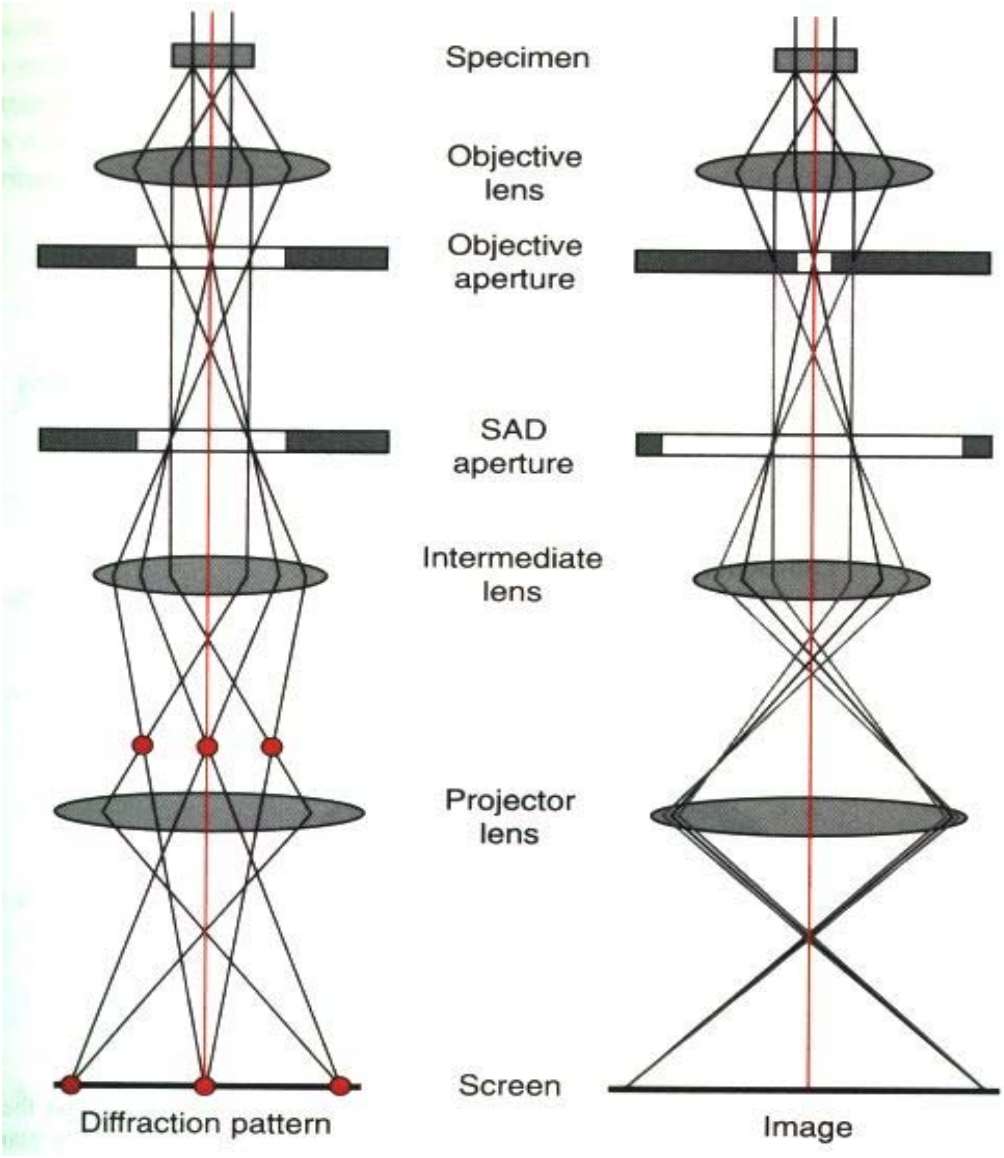

Figure 3.3: Schematic diagram of a Transmission Electron Micrograph instrument

wound clockwise. This configuration is designed to suppress noise caused by fluctuation of the large magnetic field of the superconducting magnet, and to reduce noise from the environment.

In practice, a measurement is performed by recording the output voltage of the pick up coils at a number of discrete, equally spaced positions, as the sample is drawn upward through the detection coils. To ensure that the mechanical motion of the sample transport mechanism does not cause vibrational noise in the SQUID detection system, the measurements are performed by recording the SQUID output while the sample is held stationary at a series of points along the scan length. After each scan has been completed, a mathematical algorithm is used to compute the magnetic moment of the sample from the raw data.

Since the pick-up coil is a part of a superconducting closed loop, the current induced in it will not decay over time and hence the measured flux at several positions of the specimen is independent of the motion of the sample, provided that the contribution of the environmental fields are constant over the length of measurement. Until recently, the preferred motion was a slow stepping motion through the entire pick-up coil (a "DC scan"), allowing the machine's digitizer and electronics to settle at each point. In order to reduce field variations, which are inescapable even with the best solenoid, and in order to lessen the sensitivity to environmental noise, a new measurement method, the Reciprocating Sample Operation (RSO), was designed.

To achieve highest sensitivity, a sample position is chosen to be where the response of the second order gradiometer is maximal. The sample is then oscillated vertically about this position at small amplitude, producing an output signal, which is approximately sinusoidal. The sample position, tracked through the measurement, is compared in real time to SQUID signal, yielding a phase locked measurement. The main impact of this method is the enhanced sensitivity of SQUID (1×10^{-3}emu with the RSO measurement technique).

Interpretation of magnetic measurements requires a critical state be established in the

sample. In order for the critical state to form, the field should change monotonically, and then should remain constant during the scan. If the scan length of the measurement is too long, the sample will experience a change in value of external magnetic field during the scan, because of the inhomogeneity of the field within the solenoid. Over a long scan, the sample may experience non-monotonic field variations, resulting in a reduction or even destruction of the critical state within the sample. Hence the scan length should be chosen carefully. In this work we report results obtained for a scan length of 4cm, using the DC as well as RSO measurement methods.

3.5 Mössbauer spectroscopy

Mössbauer spectroscopy[4] is a powerful tool to study the local environment of some isotopes. In this thesis, we are only interested in the Mössbauer spectroscopy of Iron nuclei. This effect utilizes the fact that a γ-ray can be emitted from a nucleus without recoil [See appendix 3A] if the nucleus is bound in the solid. In this case the emitted γ-ray has an energy separation between two states of the nucleus before and after the emission. This γ-ray can be absorbed by another nucleus of same species, by selective absorption. The isotope Co^{57} (which decays to Fe^{57}) is particularly important for the study of the local environment of Fe^{57}.

The energy scheme of Fe^{57} is shown schematically in fig.3.4 The isotope Co^{57}, which can be made by irradiation of Fe^{56} with 4MeV deuterons, decays by electron capture with a half life of 270 days to a second excited state of Fe^{57} with nuclear spin (I) equal to 5/2. It then makes a γ-transition to the first excited state with I=3/2 and finally relaxes to ground state with I=1/2, with a lifetime of 10^{-7} s. The energy separation between the last two levels is 14.4keV.

If a nucleus of Fe^{57} exist in a material then in general three distinct kind of signatures exist in the Mössbauer spectra of the sample, namely isomer shift, quadrupole splitting and Zeeman splitting.

Isomer shift [see appendix 3B for detail]: This is a shift of excited level upwards by an energy δ. One of the reasons for this shift is the small difference in the size of nucleus in

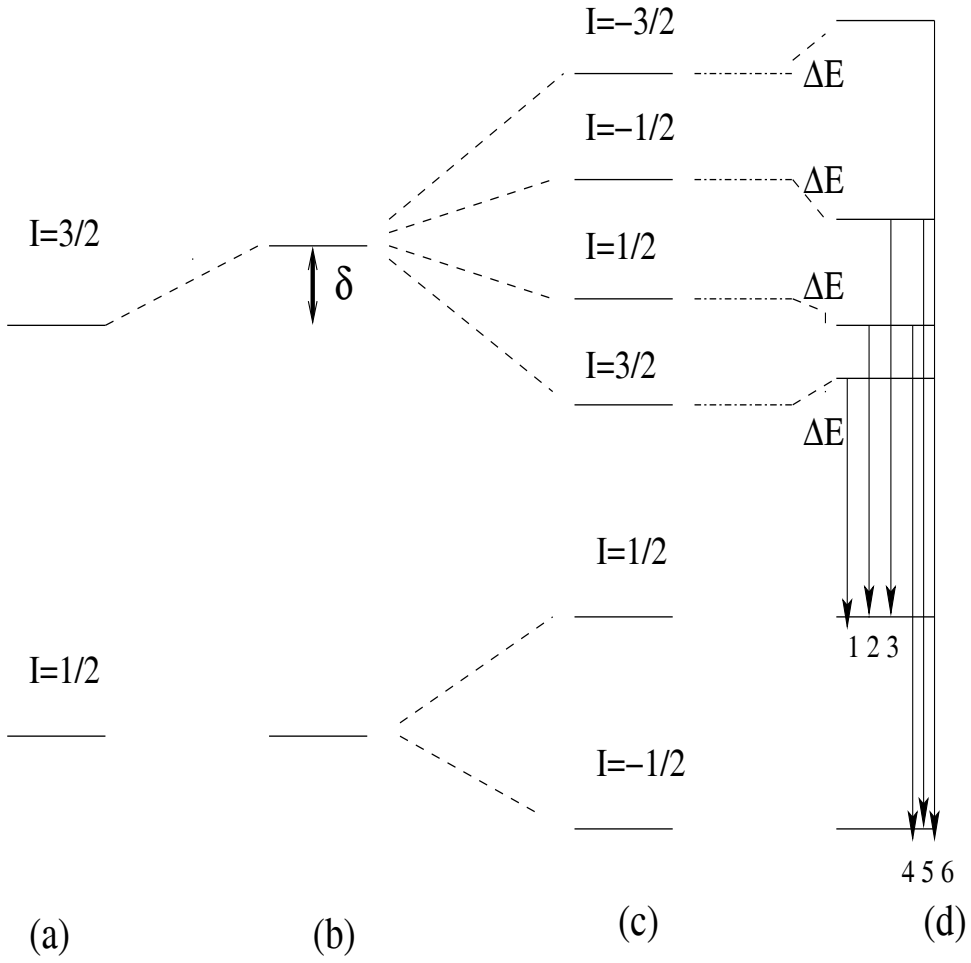

Figure 3.4: Schematic diagram of Fe^{57} nuclear energy levels (a) Unsplitted and unshifted energy levels of Fe^{57} nucleus (b) Isomer shift(δ)(c) Zeeman splitting (c) Quadrupole splitting(ΔE)

its ground state and excited state, which gives rise to differences in Coulomb interaction between the nucleus and surrounding electrons. If for some reason the electron density around the nucleus is different between emitter and absorber, the difference in coulomb interaction should result in a shift of energy levels. The isomer shift can also be caused by a difference in Debye temperature between the emitter and absorber, because the mass of the nucleus is changed during emission or absorption of γ-ray. The valence of Fe^{57} can be estimated from the isomer shift.

Quadrupole splitting [see appendix 3B for detail] : The energy levels split as shown in (fig.3.4) by the quadrupole moment of Fe^{57} in the field gradient q. No quadrupole moment exists in ground state, while the excited levels are split due to the interaction

$$\frac{1}{4}e^2qQ\frac{3\cos^2\theta - 1}{2}. \tag{3.13}$$

which leads to a spliting

$$E_{I_Z} = \frac{2e^2qQ}{I(2I-1)}[3{I_Z}^2 - I(I+1)]. \tag{3.14}$$

This sense of the splitting is positive for $I_Z = \pm\ 3/2$, while it is negative for $I_Z = \pm\ 1/2$. The sense of splitting is independent of the sign of I_Z. From this shift we can determine the field gradient and deduce the identities of the lattice sites where Fe^{57} atoms are located. This is called the quadrupole splitting.

Zeeman splitting : This splitting is the effect of internal magnetic field H_I which acts on the nucleus, the energy of the nuclear spin is given by

$$\Delta E_{I_Z} = -gM_NI_ZH_I, \tag{3.15}$$

where I_Z is the component of the nuclear spin along the direction of H_I and g is the Lande g-factor. Since I=1/2 in the ground state of Fe^{57}, the energy level is split into two 'magnetic' sub-levels with $I_Z = +1/2$ and 1/2. In the excited state with I=3/2, the level is split into four sub-levels $I_Z = +3/2$, -3/2, +1/2 and 1/2 as shown in fig.3.4. This splitting of two levels into six levels in a magnetic field causes a six finger structure in the Mössbauer spectra of a Iron nuclei in a static magnetic field, which is greater than the

natural width of the energy levels (due to life-time broadning).

3.5.1 Mössbauer Spectra in a Fluctuating Magnetic Field

Let us now consider a situation in which we attach a single domain uniaxial nanoparticle to a bath at temperature T. The giant spin of the nanoparticle, and hence the magnetic field at the nucleus then fluctuates randomly between energetically preferable easy axis directions with a fluctuation time given by the Arrhenius Kramers relation

$$\tau = \tau_0 exp(KV/k_BT), \tag{3.16}$$

where K is the magnetic anisotropy energy per unit volume of the particle, V is the volume of the particle and k_B is the Boltzmann constant. We would now like to investigate what happens to the Mössbauer line shape if we place a Mössbauer nucleus in this fluctuating field [5, 6].

The line shape of Mössbauer spectra is given by

$$I(\omega) = \frac{1}{\pi}\int_0^\infty dt e^{i\omega t - \Gamma t}\langle A^\dagger(0)A(t)\rangle, \tag{3.17}$$

where Γ is the line width of Mössbauer nuclei, and

$$A(t)(= e^{\frac{\int_0^t iH(t')dt'}{\hbar}} A(0) e^{\frac{-\int_0^t iH(t')dt'}{\hbar}}), \tag{3.18}$$

is the Heisenberg representation of the transition operator, that represents the absorption of gamma rays due to interaction between the nucleus and the radiation field. Here

$$H(t) = \mu_N g(I) I_z h(t), \tag{3.19}$$

where μ_N is the nuclear Bohr Magneton g(I) is the Lande g factor, I_Z is the projection of nuclear spin along the direction of the easy axis and h(t) is the stochastic magnetic field at the Mössbauer nuclei produced by the surrounding electronic spins. For large uniaxial anisotropy for which θ=0 and θ=π are equally likely, these spins make random transitions between the parallel and antiparallel direction of the anisotropy axis.

After a bit of algebra and using the Wigner Eckart theorem the eqn.3.17 can be written in the following form.

$$I(\omega) = \frac{1}{\pi} Re \int_0^\infty dt e^{i\omega t - \Gamma t} \sum_{m_1, m_0} \begin{pmatrix} 3/2 & 1/2 & 1 \\ m & -m_0 & M \end{pmatrix}^2 \langle e^{i\omega_{m_0 m_1} \int f(t')dt'} \rangle, \tag{3.20}$$

where m_0 and m_1 are magnetic quantum numbers of the nuclear spin in ground and excited states respectively. The triangular bracket signifies thermal average, which can be evaluated by using a two state jump stochastic process. Here $\omega_{m_0 m_1}$ equal $\mu_N h_0(m_0 g_0 - m_1 g_1)$ and f(t) is function of time which can take the values ± 1 randomly. Using this two state model we finally obtain the emission line shape expression for Mössbauer spectra as

$$I(\omega) = \frac{1}{\pi} Re \sum_{m_1, m_0} \begin{pmatrix} 3/2 & 1/2 & 1 \\ m & -m_0 & M \end{pmatrix}^2 \frac{1}{(-i\omega + \Gamma) + \frac{{\omega_{m_0 m_1}}^2}{(\lambda + \Gamma - i\omega)}}, \tag{3.21}$$

where $\lambda = \frac{1}{\tau}$.

In summary we can state that in a static magnetic field the levels are split, giving rise to the characteristic six-finger pattern. On the other hand when the field fluctuates in time rapidly around a zero mean the spectrum collapses to a single line, as though there were no magnetic field. It is important at the outset to grasp what exactly the measurement time is as far as Mössbauer spectroscopy is concerned [6]. It might seem at the first sight that it is the nuclear lifetime τ_N; however the measurement time-window is provided by the inverse of the Larmor frequencies (associated with the Zeeman interaction), and it is this which determines the line positions of the six-finger pattern. When the frequencies are larger than the relaxation rate τ one sees a static pattern whereas in the opposite limit the pattern collapses to a single line.

Appendix 3A

Basics of the Mössbauer effect

Suppose a nucleus (of mass M) moving with a velocity $\vec{V}$, in an excited state (excitation E_0 above the ground state), makes a transition to the ground state emitting a photon. Let the photon carry away an energy E (with corresponding momentum $\frac{E}{c}$ in

some direction $\hat{k}$ say). Of course the nucleus will recoil with some additional velocity $\vec{v}$.

Momentum conservation:

$$M\vec{V} = \frac{E}{c}\hat{k} + M(\vec{V} + \vec{v}) \tag{3.22}$$

and thus

$$\vec{v} = -\frac{E}{Mc}\hat{k} \tag{3.23}$$

Energy Conservation:

$$E_0 + \frac{1}{2}MV^2 = E + \frac{1}{2}M(\vec{V} + \vec{v})^2 \tag{3.24}$$

The difference of the excitation energy & the energy of the photon emitted is therefore given by:

$$E_0 - E = \frac{1}{2}Mv^2 + M\vec{V}\vec{v} \tag{3.25}$$

the first term $\frac{1}{2}Mv^2$ being the recoil energy and the second term $M\vec{V}.v$ is the energy loss due to Doppler effect (loss or gain depending on the direction of the source velocity with respect to that of the emitted photon).
The recoil energy is

$$E_R = \frac{1}{2}Mv^2 = \frac{1}{2}M(\frac{E}{Mc})^2 = \frac{E^2}{2Mc^2} \tag{3.26}$$

Because of the random thermal motion the Doppler effect will leads to a broadening of the line (the photon energy) by

$$\sim MVv \sim M\sqrt{\frac{2k_BT}{M}}\sqrt{\frac{2E_R}{M}} \sim 2\sqrt{E_RkT} \tag{3.27}$$

Photon energies from nuclear transitions have natural widths because of finite life time of the excited states (width $=\frac{h}{\tau}$ where τ is the life time). The life time for nuclear electromagnetic transition $\sim 10^{-7}$ sec. and thus the natural line width $\sim 10^{-9}$ eV.

These considerations are important in considering the possibility of resonant absorption which is the process whereby a photon of energy E emitted by a nucleus in an excited

state (excitation energy E_0) can be absorbed resonantly by a nucleus of the same species (making a transition from the ground state to the excited state of excitation E_0).

The main issue here is whether or not the off set caused by the recoil can be made up by the broadening provided by the natural width & the Doppler effect due to thermal motion.
In the case of nucleus typically $E \sim 100$ keV. Thus

$$E_R \sim \frac{E^2}{Mc^2} \sim \frac{100 \times 10^3 eV}{2 \times (100 \times 10^9) eV} \;\; 100 \times 10^3 eV \sim \frac{1}{2} \times 10^{-3} eV \tag{3.28}$$

Which is a **huge off-set** by the standards of the natural width ($\sim 10^{-9}$eV) or the Doppler broadening $\sim 10^{-5}$eV at room temperature.

In 1956 & 1957 R.L. M*ö*ssbauer was studying the scattering of gamma rays at the Max Plank Institute in Heidelberg. While comparing the scattering of 129 keV gamma rays of ^{191}Ir produced by that nucleus bound in a solid & absorbed by ^{191}Ir in a solid, he found to his amazement that there was an **Increase** in scattering as the temperature was **Lowered**. [One would have expected, if at all, the very opposite to happen (viz. an **Increase** in scattering) as the temperature was **Raised**, due to Doppler broadening, to compensate for the energy loss due to recoil]. The interpretation of this apparently paradoxical result marks the beginning of the **M*ö*ssbauer Effect**.

The central idea was that for a nucleus embedded in a solid there was a probability of **Recoil-less** emission of gamma ray (the Debye-Waller factor).

The emission of the photon of the energy E (& wave number k: $hk = \frac{E}{c}$) involves the plane wave $e^{i\vec{k}.\vec{r}}$, where $\vec{r}$ is the centre-of-mass coordinate of the nucleus. To calculate the probability that the transition occurs without recoil requires us to calculate temperature averaged matrix element

$$<< nw_j|e^{i\vec{k}.\vec{r}}|nw_j >> \tag{3.29}$$

viz. the probability that the state of the solid lattice characterized vide the occupancies of states specified by the various phonon frequencies w_j (upto the Debye frequency w_D)

remains unaltered (hence the diagonal matrix elements with phonon numbers) & then averaged over thermal distribution corresponding to the given temperature.
The final result for $T << \theta_D$ (the Debye temperature) is

$$f = exp[-\frac{E_D}{k\theta_D}(\frac{3}{2} + \frac{\pi^2 T^2}{\theta_D^2})] \tag{3.30}$$

which is the Debye-Waller factor, expressing the fraction of gamma-ray emission or absorption taking place without recoil. For a heuristic discussion of this Debye-Waller factor [9]. For 14.4kev gamma of ^{57}Fe we have f ~ 0.91 for liquid nitrogen temperature. Of course for large energy gammas f does fall off rapidly.

Accordingly a new and powerful tool opens up for measuring very very small shifts in nuclear levels

- with recoil-less gamma transition made possible by the Mössbauer effect.
- with the natural widths $\sim 10^{-8} ev$.
- using resonance absorption employing Doppler effect vis a vis moving source or absorber by a drive moving at some velocity V.

caused by say
Isomer Shift.
environmental effect vide quadrupole moment or hyperfine splitting & so on

Doppler drive with a velocity V to compensate small differences in energy of the order of the natural line-width ($\sim 10^{-9} eV$) may easily be estimated by requiring that $\frac{1}{2}MV^2$ (taking M to be say 100 Daltons) will lead to $\frac{V}{c} \sim 10^{-10}$. Thus a Doppler drive moving at the rate of millimeters per second is adequate.

Appendix 3B

Isomer Shift and Quadrupolar Splitting

Mössbauer spectroscopy enables the determination of small shifts and splittings of nuclear energy levels. Of particular importance is the effect of the environment of atoms and molecules around a "Mössbauer nucleus". Clearly this interaction will be electromagnetic in nature and we shall focus our attention on the electrostatic effects of the surrounding leading to the isomer shift and quadrupolar splitting. The effect of magnetic field has been discussed in the text.

Consider the nuclear charge distribution $\rho(\mathbf{r})$ [taking the origin here and elsewhere at the center of the nucleus] placed in an electrostatic potential$\phi(\mathbf{r})$ due to the extranuclear charges present in the environment, the corresponding electric field due to which is $\mathbf{E} = -\nabla\phi$. The energy of the nuclear charge distribution in this "external" field is then given by

$$U = \int d^3\mathbf{r}\rho(\mathbf{r})\phi(\mathbf{r}) \tag{3.31}$$

Let us make a Taylor series expansion of $\phi(\mathbf{r})$ around the point $\mathbf{r} = \mathbf{0}$ (the origin), namely

$$\begin{aligned}\phi(\mathbf{r}) &= \phi(\mathbf{0}) + \sum_i x_i \left(\frac{\partial\phi}{\partial x_i}\right)_{\mathbf{r}=\mathbf{0}} + \frac{1}{2!}\sum_i\sum_j x_i x_j \left(\frac{\partial^2\phi}{\partial x_i \partial x_j}\right)_{\mathbf{r}=\mathbf{0}} + \cdots \\ &= \phi(\mathbf{0}) - \sum_i x_i \left(E_i\right)_{\mathbf{r}=\mathbf{0}} - \frac{1}{2}\sum_{i,j} x_i x_j \left(\frac{\partial E_j}{\partial x_i}\right)_{\mathbf{r}=\mathbf{0}} + \cdots \end{aligned} \tag{3.32}$$

Inserting this expression for $\phi(\mathbf{r})$ in the expression for the interaction energy U we obtain

$$U = [\int d^3\vec{r}\rho(\vec{r})]\phi(\vec{0}) - \sum_i [\int d^3\vec{r}\rho(\vec{r})x_i]E_i(\vec{0}) - \sum_{i,j}[\frac{1}{2}\int d^3\vec{r}\rho(\vec{r})x_i x_j]\frac{\partial E_j(\vec{0})}{\partial x_i} + \cdots$$

The quantities in square brackets pertain to the nuclear charge distribution and these are multiplied (or contracted) with field quantities that characterize the electrostatic potential due to the surroundings. The expression is rapidly convergent as the "size" of the

nuclear charge distribution is small (of the order of femtometers) as compared to the typical distances (Angstroms) over which the electrostatic potential due to the environment varies. Thus the first term in the expression $U_0 \equiv [\int d^3\vec{r}\rho(\vec{r})]\,\phi(\vec{0})$ is simply the total charge of the nucleus multiplied by the electrostatic potential due to the surroundings at the center of the nucleus. It simply represents a shift in the energy. It is this term which is responsible for the **Isomer Shift** to be discussed later.
The second term $U_1 = \sum_i [\int d^3\vec{r}\rho(\vec{r})x_i]\,E_i(\vec{0}) = \sum_i E_i(\vec{0})p_i = -\mathbf{p_i}.\mathbf{E}$ is the interaction of the electric dipole moment $\int \rho(\vec{r})\mathbf{p}d^3\vec{r}$ with the net electric field due to the environment. In quantum mechanics this would imply replacing $\int \rho(\vec{r})\hat{\mathbf{p}}d^3\vec{r}$ by $\langle\psi|e\vec{r}|\psi\rangle$ as $\rho = \psi^*\psi$. However, since $\mathbf{p} = \mathbf{e\vec{r}}$ is a parity odd operator (viz. $\vec{r} \to -\vec{r}$ under spatial inversion) we will have $\langle\psi|e\vec{r}|\psi\rangle = 0$ and thus the second term is irrelevant for our purpose.

Now take the third term in the expansion,

$$U_2 = -\sum_{i,j}\left[\frac{1}{2}\int d^3\vec{r}\rho(\vec{r})x_ix_j\right]\frac{\partial E_j(\vec{0})}{\partial x_i} = -\frac{1}{2}\sum_{i,j}\frac{\partial E_j(\vec{0})}{\partial x_i}\int d^3\vec{r}\rho(\vec{r})x_ix_j \tag{3.33}$$

Now since the sources producing the electric field $\mathbf{E}$ are external to the nucleus, we have the Laplace equation

$$\nabla.\mathbf{E} = \sum_i \frac{\partial E_j(\vec{0})}{\partial x_i} = \sum_{i,j}\frac{\partial E_j(\vec{0})}{\partial x_i}\delta_{ij} \tag{3.34}$$

Accordingly we may write

$$U_2 = -\frac{1}{2}\sum_{i,j}\frac{\partial E_j(\vec{0})}{\partial x_i}\int d^3\vec{r}\rho(\vec{r})\left(x_ix_j - \frac{1}{3}r^2\right) \tag{3.35}$$

as the additional term inserted by us makes no contribution by virtue of the Laplace equation. This we rewrite as:

$$U_2 = -\frac{1}{6}\sum_{i,j}\frac{\partial E_j(\vec{0})}{\partial x_i}\int d^3\vec{r}\rho(\vec{r})\left(3x_ix_j - r^2\delta_{ij}\right) \tag{3.36}$$

$$= -\frac{1}{6}\sum_{i,j}Q_{ij}\frac{\partial E_j(\vec{0})}{\partial x_i} \tag{3.37}$$

where $Q_{ij} = \int d^3\vec{r}\rho(\vec{r})\,(3x_ix_j - r^2\delta_{ij})$
This Q_{ij} represents the **Electric Quadrupole Moment** which is a tensor of rank 2.

So U_2 gives the quadrupole contribution to the energy of the charge distribution, the quadrupole being assumed to be located at the origin (i.e. it is actually the quadrupole moment of the nucleus).

So we find that the quadrupole contribution to the energy due to the interaction of the Electric Quadrupole moment of the nucleus (which is a second rank tensor) with the Electric Field Gradient (the external EFG, which is also a second rank tensor).

Now again in Quantum Mechanics, $\rho(\vec{r}) = |\psi|^2 =$ the probability density $= \psi^*\psi$. So one is concerned here with the expectation values of various operators. The electric quadrupole moment eQ is defined in terms of the expectation value of the operator $(3z^2 - r^2)$

$$eQ = \langle J, M = J \left| (3z^2 - r^2) \right| J, M = J \rangle \tag{3.38}$$

We take the matrix element of the operator $(3z^2 - r^2)$ between the the angular momentum state characterizing the nucleus with the magnetic projection $M = J$. The other matrix element will simply be related to this through "geometric" factors (viz. the Clebsch-Gordan coefficients). The quadrupole moment operator $(3z^2 - r^2)$ can be written as $\sqrt{\frac{16\pi}{5}} Y_2^0 = {Q_2}^0$ corresponding in term of the spherical harmonic the zeroth component of the quadrupole tensor. To calculate the quadrupole splitting, one has to calculate the diagonal matrix elements (i.e. expectation values) between the angular momentum eigenstates. In order to do so; we now use a trick! We note that the spherical harmonics, and thus in turn Q_2^m $(m = -2, \cdots +2)$, are second rank irreducible spherical tensors. Now the operators $\hat{J}^2, \hat{J}_z^2, \hat{J}_z\hat{J}_\pm, \hat{J}_\pm\hat{J}_\pm$ are also second rank rank tensors. So we try to link the Q_2^m's in terms of the above quantities. The advantage of this is that one can then straight away write down the matrix elements from our knowledge of angular momentum theory in quantum mechanics otherwise we would have to use the machinery of Racah-Wigner algebra, and in particular the Wigner-Eckart Theorem and Clebsch-Gordan coefficients. Now

$$Q_2^0 = 3z^2 - r^2 \equiv \frac{\alpha}{2}\left(3\hat{J}_z^2 - \hat{J}^2\right) \tag{3.39}$$

where α is some constant which has to be determined.

Now we have to fix the value of α

$$eQ \;\; = \;\; \left\langle J, M = J \left| Q_2^0 \right| J, M = J \right\rangle$$

$$\begin{aligned} &= \left\langle J, M = J \left| \frac{\alpha}{2} \left(3\hat{J}_z^2 - \hat{J}^2 \right) \right| J, M = J \right\rangle \\ &= \frac{\alpha}{2} J \left(2J - 1 \right) \end{aligned} \tag{3.40}$$

So that

$$\alpha = \frac{2eQ}{J(2J-1)} \tag{3.41}$$

So now we can write down the Hamiltonian of interaction between the EFG (Electric Field Gradient) and the quadrupole moment Q as

$$\begin{aligned} H &= -\left(\frac{\partial E_z}{\partial z} \right) \left(3z^2 - r^2 \right) \\ &= \frac{eq\alpha}{2} \left(3\hat{J}_z^2 - \hat{J}^2 \right) \end{aligned} \tag{3.42}$$

So finally,

$$H = \frac{2e^2qQ}{J(2J-1)} \left(3\hat{J}_z^2 - \hat{J}^2 \right) \tag{3.43}$$

Isomeric Shift

It is worthwhile looking more closely at the first term in the expansion of the energy of the nucleus in the electrostatic field due to the surrounding, viz., the monopole contribution. This causes a shift in the energy without causing any splitting. Why is this interesting? Consider a nucleus surrounded by and penetrated by the electronic charges around it – a uniform charged sphere (let us say) embedded in its s-electron charge cloud (only the s-electron, viz., those with orbital angular momentum quantum number l=0 will be non-vanishing near $r = 0$ as the wavefunction $\psi \sim r^l$ for small r). A difference in the s-electron density (caused say by a change in valence between the iron compound in the emitter and the absorber) would manifest in a relative shift in the nuclear energy levels which should be called electric monopole shift in analogy with electric quadrupole splitting but this is uniformly referred to as "isomer shift" [10, 11].

To make an estimate of the energy shift let us consider a very simple model of the nucleus as a uniformly charged sphere of radius R. The energy shift as compared to what it would be if the nucleus were a point charge is given by:

$$\delta E = -e \int_0^\infty |\psi|^2 (\phi - \phi_{\text{point-charge}}) d^3\vec{r},$$

where ϕ due to this uniformly charged sphere is $\frac{Ze}{r}$ for $r \geq R$ and $\frac{Ze}{R}[\frac{3}{2} - \frac{r^2}{2R^2}]$ for $r \leq R$, while $\phi_{\text{point-charge}} = \frac{Ze}{r}$ everywhere. Accordingly,

$$\delta E = -e \int_0^R |\psi|^2 [\frac{3}{2} - \frac{r^2}{2R^2}] 4\pi r^2 dr \approx |\psi(0)|^2 \frac{2\pi}{5} Ze^2 R^2$$

where in the last step we have taken the electronic wavefunction $\psi(r)$ to be essentially a constant viz. $\psi(0)$ inside the small nucleus of radius R...small by the standards of the electronic wavefunction. Now R will generally be different for the ground and excited states of the nucleus so that even if the emitter and the absorber nucleus had their surrounding electrons in the same state there would be an isomer shift given by

$$\delta E_{\text{ex}} - \delta E_{\text{gd}} = \frac{2\pi}{5} Ze^2 |\psi(0)|^2 (R_{ex}^2 - R_{gd}^2),$$

Where R_{ex} and R_{gd} are the nuclear radius in the excited and ground state respectively. If, however, the valence state of the electrons in the source and absorber were different then the isomer shift would be given by:

$$\frac{2\pi}{5} Ze^2 [|\psi_{\text{absorber}}(0)|^2 - |\psi_{\text{source}}|^2][R_{\text{ex}}^2 - R_{gd}^2]$$

Bibliography

[1] C. Kittel, *Introduction to Solid State Physics* (John Wiley & Sons, USA)

[2] B. D. Cullity, *Elements of X-ray Diffraction*(1978).

[3] A fantastic review of this subject is given in the book by M.D. Graef *Introduction to Conventional Transmission Electron Microscopy*(Cambridge University Press, 2003)

[4] Soshin Chikazumi, *Physics of Ferromagnetism* (Oxford university press, UK, 1997)

[5] S. Dattagupta in Mössbauer Effect: Application to Physics, Chemistry and Biology, (B. V. Thosar, P. K. Iyengar, J. K. Srivastava and S. C. Bhargava, eds.) Elsevier, Amsterdam, 1983.

[6] S. Dattagupta, in *Mössbauer Spectroscopy in Perspectives* (F. J. Berry and D. P. E. Dickson, eds.) Cambridge University Press, London and New York, 1986; also in Hyperfine Interaction **49**, 253 (1989).

[7] F.R. Mentzger, Prog. Nucl. Phys. **7** (1959) 53

[8] K.G. Malmfors, "Beta and Gamma Spectroscopy" Ed. Kai Sigbahn.

[9] Harry J. Lipkin, Annals of Physics **23** (1963) 28

[10] Kistner and Sunyar, Phys. Rev. Lett.**4** (1960) 412

[11] Melissinos and Davis, Phys. Rev. **115**(1959) 130

Chapter 4

The effect of a weak ferromagnetic matrix on a system of nanomagnetic particles

Systems of magnetic nanoparticles have been gaining increasing attention over the past few years both because they introduce novel physical concepts and because of their vast potential for applications in the fields of nano-electronics, storage media and medicine [1, 2, 3, 4, 5, 6, 7]. For practical devices, the nanoparticles are usually imbedded in a matrix or placed on a solid substrate. The influence of different background materials on the magnetic properties of the nanoparticle system is a relatively open topic. Though it is clear that different materials can have various effects on the magnetic coupling between the particles (depending on the magnetic nature of the matrix in which they are embedded) a full understanding of these issues is lacking.

Previous theoretical and experimental studies have discussed the effect of interactions on the magnetic properties of nano-magnetic particles. In this chapter we study a unique kind of interaction effect where the system acts like a "Super-SpinGlass" system in the presence of a very weak external magnetic field (H), but this interaction becomes ineffective at H=0. This observed result can not be explained by using existing models. We compare the magnetic behavior of Ni nanoparticles embedded in gold (a diamagnetic material) to that of Ni particles embedded in graphitic carbon which has been shown to exhibit weak ferromagnetic properties [8, 9]. The latter exhibits a set of surprising and contradictory findings. These are attributed to the coupling between the nanomagnetic particles via the weak ferromagnetic material in the presence of a small magnetic field. We show that this is a unique case in which the magnetization and blocking temperature

[1](T_B) of the system strongly depend on whether a small external field is applied.

The synthesis of Ni-C (graphitic) core-shell nanostructures was carried out by thermal dissociation of nickel acetylacetonate, $Ni(C_5H_7O_2)2$, in a closed vessel cell assembled from stainless steel Swagelok parts. The full process is described elsewhere [10]. Due to the lack of a commercially available gold precursor to carry out a similar synthesis, we produced Ni-Au core-shell using a two step process. At first, the nuclei of Ni nanoparticles were formed in a solution of nickel (II) acetate tetrahydrate [99.998, Aldrich Chemical Co.] in EG (Ethylene glycol). A 100mL glass flask was placed in a microwave oven (spectra 900W) that was connected to the water condenser. Some 50 mL of a solution of 0.2M $Ni(Ac)_2$ in EG was purged by argon for 10 min, after which the microwave oven was turned on at the power level of 60 watt with a continued flow of the argon gas. A black suspension appeared after 15 minutes of microwave irradiation. In the second stage, 0.15mL chloroauric acid ($HAuCl_4$) was added by a microliter size syringe (Hamilton Co.) in the black suspension of Nickel nanoparticles. Once again microwave irradiation was turned on and maintained for 20 minutes at a power of 60 watt. The resulting pale-black solid product was washed thoroughly with ethanol thrice and centrifuged at 8000 rpm. The as-prepared product was dried in a vacuum chamber for 12 hours.

The morphology and crystal structure for both samples were studied by TEM [2]and HR-TEM. Figure 4.1a depicts the TEM analysis of a Ni nanoparticle (with sizes ranging from 30-150nm) embedded in graphitic carbon. The image shown in the top right inset confirms the formation of ordered graphitic carbon shell of 15nm. The interlayer spacing between these graphitic planes is 3.41 Å, which is very close to that of the graphitic layers. The image in the bottom right inset provides further verification for the identification of the core as Ni. It illustrates the perfect arrangement of the atomic layers and the lack of defects. The measured distance between these (111) lattice planes is 0.200 nm, which is very close to the distance between the planes reported in the literature (0.203 nm) for the face-centered cubic lattice of the Ni ((PDF No. 03-065-2865).

The TEM analysis of Ni particles (sizes of 100-200nm) coated by gold nanocrystals with diameters of 7nm is shown in Figure 4.1b. The inserted (HR-TEM) top image

[1]see chapter2

[2]see chapter 3

confirms the interlayer spacing for Au nanocrystals and the bottom image provides further evidence for the Ni core.

Figure4.2 depicts the field cooled - zero field cooled (FC -ZFC) magnetization measurements for the Ni-C and Ni-Au samples as measured in a SQUID magnetometer. In ZFC mode the system is cooled to the lowest temperature in the absence of magnetic field (H), and the magnetization M(T) is measured while heating the sample in the presence of H=100 Oe, while in FC, M(T) is measured during cooling the sample in the presence H=100 Oe. For superparamagnetic systems the ZFC magnetization curves are expected to show a peak corresponding to the average blocking temperature while the FC curves always increase as the temperature is decreased due to the alignment of the spins in the direction of the field. Our measurements show that for the Ni-Au system T_B is found to be of the order of 150 K (which is a reasonable value for Ni particles with diameters of 150 nm). Since the Ni particles in the carbon coated systems are smaller, the average blocking temperature is expected to be smaller as well (a rough estimation yields $\sim 30K$). Surprisingly, for the Ni-C case the blocking temperature is found to be well above 400 K (which was the highest available temperature). Moreover, the temperature dependance of the magnetization in these samples is very peculiar. The FC C-Coated Ni particles exhibit magnetization that remains almost constant even down to temperatures of 15 K.

Another peculiarity of these systems is demonstrated in fig.4.3 which depicts the low-field regime of the room temperature M-H curves of both samples. It is seen that the coercive field, H_C is *smaller* for the carbon coated sample ($\sim 60Oe$) than that of the gold coated sample ($\sim 170Oe$). This seems to be in striking contradiction to the fact that the blocking temperature extracted from the FC-ZFC measurements is much larger for the Ni-C sample.

An even more surprising finding is related to relaxation-response measurements below the blocking temperature. In this measurement, the sample is cooled to a temperature of 40 K (well below the measured T_B for both types of samples) in the absence of magnetic field. At this temperature a 50 Oe field is abruptly switched on and the magnetization is measured as a function of time. After a few hours the field is switched back off and the M(t) is measured again. Figure 4.4 compares the relaxation-response measurements for the Ni-Au and Ni-C samples. It is seen that the Au coated Ni sample shows slow response

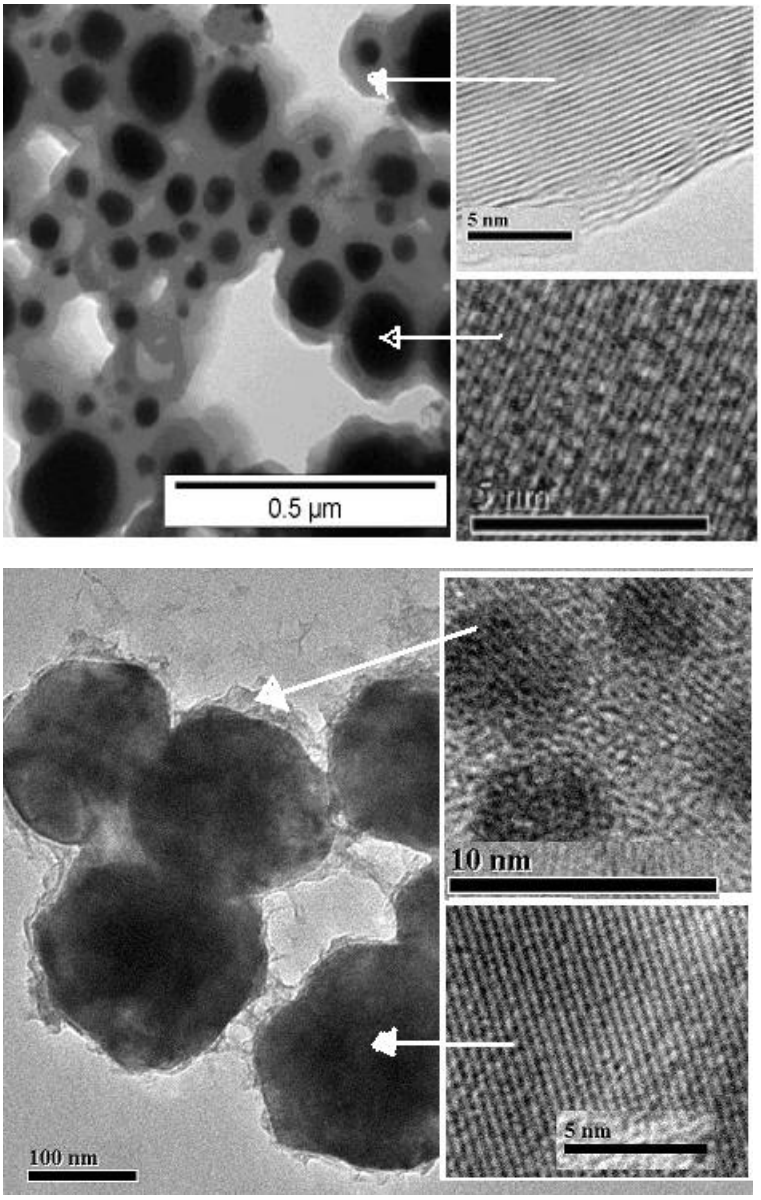

Figure 4.1: Transmission electron micrographs of (a) Ni nanoparticles embedded in graphitic carbon, and (b) Ni particles coated by gold nanocrystals. The left panels are conventional low magnification TEM images and the right panels are high resolution TEM images taken at different sections of the samples.

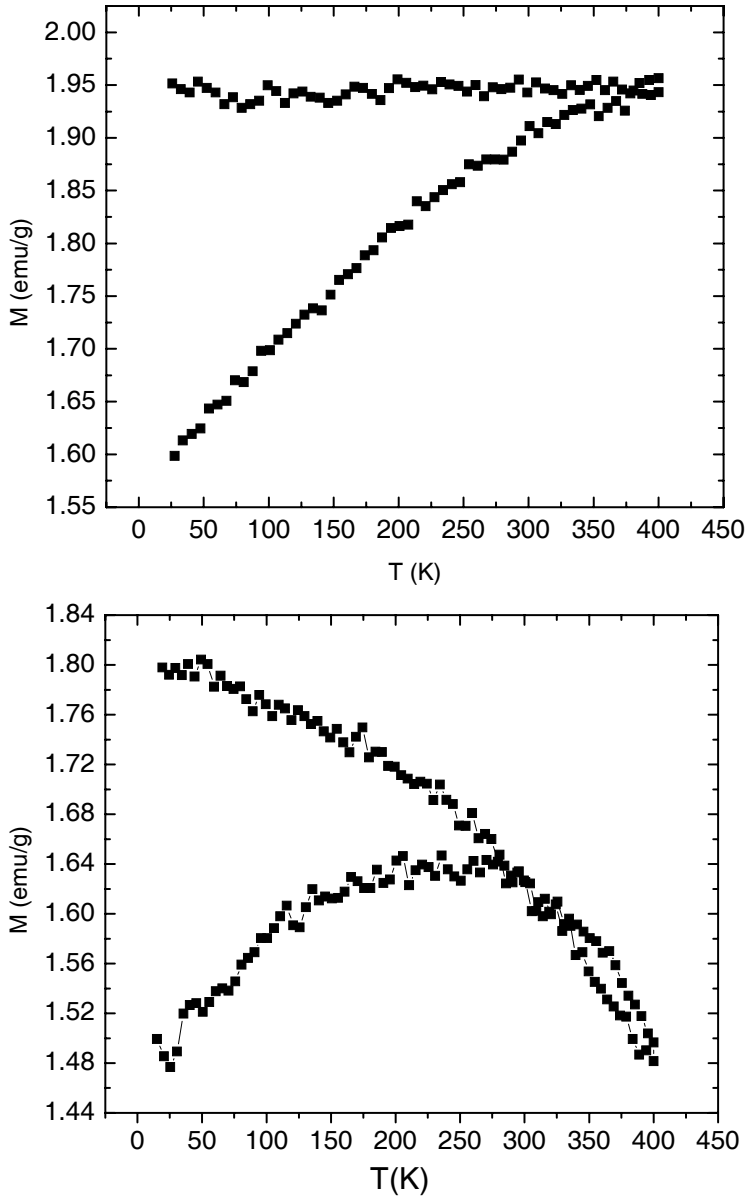

Figure 4.2: FC and ZFC M(T) plots for Ni-C (top) and Ni-Au (bottom) nanoparticle systems.

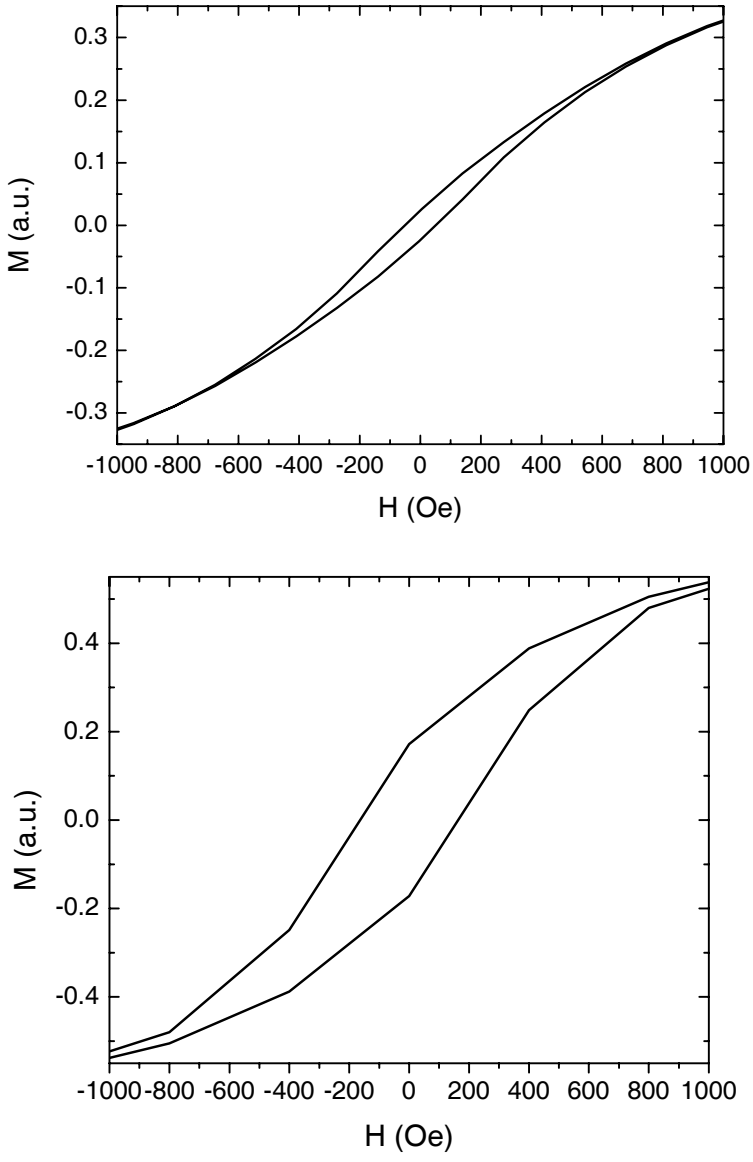

Figure 4.3: Room temperature hysteresis loops for the Ni-C (top) and the Ni-Au (bottom) samples

to changes in the external magnetic field. When the field is switched on the magnetization increases slowly and when it is switched back off there is a long time associated with the magnetization decay. This is expected because the magnetic orientation of a particle is blocked at temperatures smaller than T_B . The Ni-C sample, on the other hand, responds almost immediately (within the measuring time scale of SQUID) to the magnetic field changes. Upon switching the field off the magnetization drops immediately to zero and upon switching the magnetic field back on the magnetization is restored to its maximal value instantaneously. This behavior is very unexpected for a system of particles with blocking temperatures above 400 K.

In an attempt to understand the results observed in the Ni-C samples we considered the possibility that the observed large blocking temperatures are due to dipole-dipole interactions between the magnetic moments of the Ni-nanoparticles (super-spin-glass behavior [11]) mediated by the ferromagnetic background. To check the relevance of this mechanism in our system we performed arrested cooling ZFC measurements. In this experiment the system is cooled in the absence of magnetic field from room temperature to 30 K (well below the T_B of the system) and the temperature is arrested for four hours. Then the system is cooled again at a constant rate to 15 K in the absence of the external magnetic field. From 15 K the sample is heated up to room temperature in the presence of 50 Oe DC external magnetic field, while monitoring the magnetization constantly. An established sign of super-spin-glass interactions [11] is the occurrence of a dip in the M-T heating curve at the temperature that was arrested during the cooling process (30 K in our case). Our Ni-C samples showed no sign of such a dip, thus ruling out the existence of pronounced spin glass interactions.

Nevertheless, the fact that the puzzling (and apparently contradictory) results were not observed in the Ni-Au systems leads us to suggest that this unique phenomenon is due to interparticle (Ni-Ni) interaction mediated via the weak ferromagnetic carbon matrix. In the following paragraphs we suggest a model, based on such interactions, that may account for our experimental findings.

Let us consider an assembly of Ni nanoparticles coated by graphitic carbon, in which the easy axis of the Ni-particles are randomly oriented. The carbon coating is characterized by very weak ferromagnetism. Let E_{nn} be the magnetic interaction between the

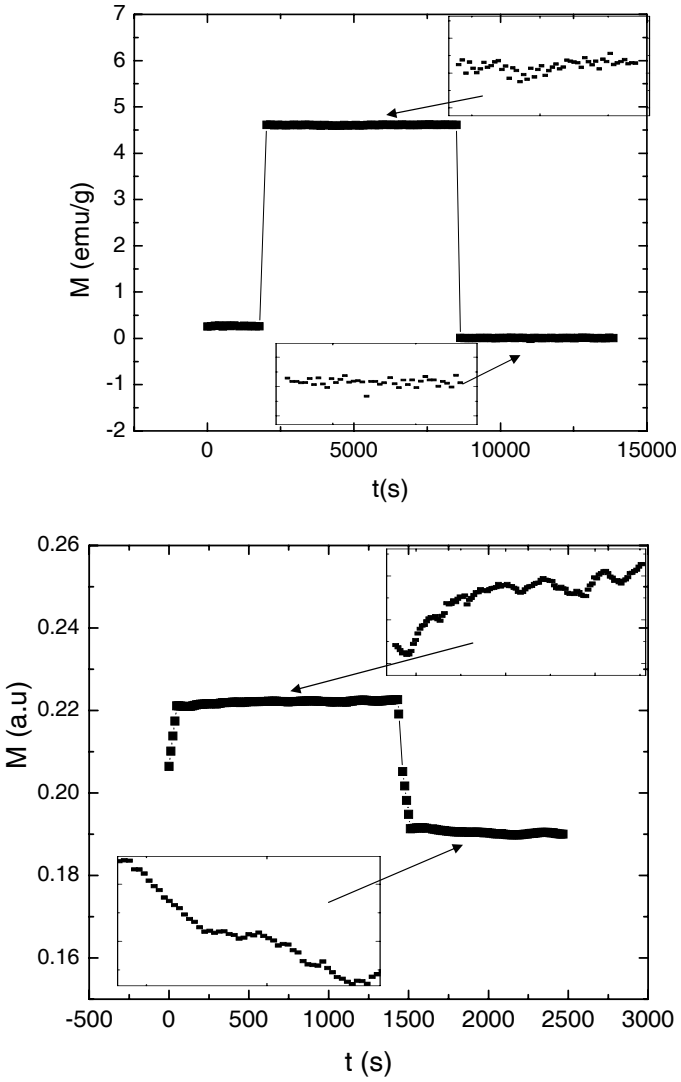

Figure 4.4: Relaxation response graphs for Ni-C (top) and Ni-Au (bottom) nanoparticle systems.

atoms of Ni, E_{nc} the interaction between Ni and C and E_{cc} the interaction energy between carbon atoms. The dipolar interaction between Ni-nanoparticles is assumed to be weak due to small Ni particle size and large inter-particle separation. Let us further assume that $E_{nc} >> E_{cc}$. In the absence of magnetic field there is a spin disorder in the carbon shell coating the Ni particle due to the surface spin disorder of the Ni particles [12] and the random orientation of the easy axis. But as soon as an external magnetic field is applied, all the Carbon spins orient themselves in the field direction, producing a huge effective magnetic field on the Ni-nanoparticle, H′, thus forcing it to orient along the external field direction.

The apparent contradiction observed for Ni-C samples occurs due to the fact that two different classes of experiments (namely field measurements and zero field measurements) were compared. FC-ZFC belongs to finite applied field measurements while relaxation measurements belong to zero field measurements. Taking this fact into account, our experimental observations can be well explained within the framework of the above model. Let us first discuss the FC-ZFC measurement. Consider a single domain uniaxial magnetic nanoparticle. The anisotropy energy of such a particle is given by:

$$E = KVsin^2\theta \tag{4.1}$$

where K is the anisotropy energy per unit volume, V is the volume of the nanoparticle and θ is the angle between the magnetic moment of the particle and the easy axis for magnetization. In absence of an external magnetic field the probability of finding an up spin is equal to that of a down spin, leading to zero magnetization. If the temperature of the system is decreased in absence of the external magnetic field the situation remains the same and zero magnetization is observed. As soon as an external magnetic field is applied the energy of the system becomes

$$E = KVsin^2\theta - \mu VH^{\star}cos\theta \tag{4.2}$$

where μ is the magnetic moment of the particle per unit volume and $H^{\star} = H + H'$ is the effective magnetic field seen by the particle due to external magnetic field and the field produced by surrounding Carbon spins. In eq. 4.2 we have assumed, for simplicity, that the external magnetic field is applied along the direction of easy axis of the nanoparticle.

Let δE_{0m} be the energy difference between the minima at $\theta = 0$ and that of the maxima E_m, and δE_{1m} be that between the energy at $\theta = \pi$ and E_m. Due to the contribution of large number of Carbon spins, $H^\star$, is extremely large. This leads to $\delta E_{0m} \gg \delta E_{1m}$, which means that with increasing temperature the down spin will easily orient parallel to the applied magnetic field with the help of thermal energy. The magnetization can decrease with increasing temperature only if the thermal energy becomes comparable to δE_{0m}, which is a very high value. Hence, unusually large effective blocking temperature are measured by the ZFC magnetization experiment. If now the system is cooled in the presence of an external magnetic field, the particles are already blocked along the direction of external field and the FC curve becomes independent of temperature.

The magnetization response measurement are also understood using the above considerations. As soon as the magnetic field is switch on the system's Hamiltonian becomes that of eq. 4.2. Since $H^\star$ produces a large asymmetry in the energy profile. In this case the response time (the time it takes for the spins to flip along the external field) given by:

$$\tau = \tau_0 \exp\left[\frac{KV \sin^2(\theta) + \mu V H^\star cos(\theta)}{K_B T}\right] \tag{4.3}$$

is very short compared to that of the Ni-Au samples in which the magnetic field is much smaller.

The magnetization relaxation measurement, on the other hand, is a zero field magnetic measurements. In effect these systems are characterized by two distinct blocking temperatures; a zero field, conventional blocking temperature, $T_B(0)$, and a finite field blocking temperature $T_B(H)$, which is much larger due to the effect of the carbon atoms. When the magnetic field is switched off, the carbon spins disorient immediately. Since $T_B(0)$ of the Ni particles is estimated to be a few tens of degrees, at 40K they behave as isolated nano-magnets with a small barrier height. Hence, fast relaxation is expected. This is in vast contradiction to the situation for the FC-ZFC measurements in which a field is applied and the finite field blocking temperature, $T_B(H)$, determines the magnetization properties. A similar argument is related to the coercive field, H_C which is the field associated with zero magnetization. Since very small external magnetic fields are sufficient to align the orientation of the grains, thus giving rise to large measured magnetization, the field for which zero magnetization is achieved in the Ni-C samples is expected to be very

low.

In conclusion we note that we have introduced the idea of a unique type of interaction which is active only in presence of an applied magnetic field. In a system of magnetic nano-particle with such type of special back ground, in first sight with field measurements it may appear that the system behaves like a "Super-SpinGlass" system. But systematic characteristic measurement protocols for "Super-Spinglass" systems: like arrested ZFC measurement leads us to conclude that this "Pseudo-Super-SpinGlass" behavior is effective only in presence of an applied field. The non-interacting nature in the absence of an applied field is confirmed from the zero-field relaxation behavior of the system, at temperature well below the blocking temperature in field measured experiments.

Bibliography

[1] A.N.Goldstein, *Hand Book of Nanophase Materials*, New York:Marcel Dekker Inc. (1997).

[2] R.H. Kodama, J. Magn. Magn. Mater., **200**, 359 (1999).

[3] *Magnetic Properties of Fine Particles*, edited by J.L.Dormann and D.Fiorani, North-Holland, Amsterdam (1992).

[4] K.M.Unruh and C.L.Chein, *Nanomaterials:Synthesis,Properties and Applications* edited by A.S.Edelstein and R.C.Cammarata, Bristol: Institute of Physics.

[5] I.S.Jacobs and C.P.Bean in *Magnetism III* (eds.) G.T.Rado and H.Suhl, (New York: Academic)(1963).

[6] *Physical principles of Magnetism*, A.H. Morrish, John Wiley, New York, 1965.

[7] S.H. Sun, *et-al*, Science **287**, 1989 (2000).

[8] T. L. Makarova, B. Sundqvist, R. Hohne, P. Esquinazi, Y. Kopelevich, ; P. Scharff, V. A. Davydov L. S. Kashevarova, and A. V. Rakhmanina, Nature , **413**, 716 (2001).

[9] A. A. Ovchinnikov, and I. L. Shamovsky, THEOCHEMs-J. Mol. Struct., **83**, 133 (1991).

[10] S.V. Pol, V.G. Pol, A. Frydman, G. N. Churilov, and A. Gedanken, Journal of Physical Chemistry, in press.

[11] M.Sasaki, P.E.Jonsson, H.Takayama and P.Nordblad, Phys. Rev. Lett. **93**, 139701 (2004).

[12] R.H. Kodama, A.E. Berkowitz, E.J. McNiff, Jr., and S. Foner, Phys. Rev. Lett. **77**, 394, (1996).

Chapter 5

Tuning the relaxation dynamics of nano-magnets via magnetization

Interest in magnetic nano-particles has increased in the past few years not only because of their application in ultra high density recording etc but also their relevance in fundamental physics issues. Most applications rely on the stability of magnetic order of nano-particles with time. However with decreasing particle size magnetic anisotropy energy per particle responsible for holding the magnetic moment along certain directions becomes comparable to thermal energy. Thermal fluctuations then induce random flipping of the magnetic moments with time, and the particles lose their magnetic order and become superparamagnetic[1, 2, 3, 4, 5, 6, 7, 8, 9, 10, 11, 12]. This thermal relaxation dynamics can be tuned by changing the particle size, anisotropy energy and inter-particle separation (interaction). A large body of work has been carried out to study the effect of particle size and inter-particle interaction [13, 14, 15, 16, 17, 18, 19]. However, increasing the volume of the particle to increase the stability is not desirable for memory devices, since space minimization is one of the necessary criteria for these devices. Interparticle interaction adds further complications. In this chapter we show how the magnetization of the nanomagnets can be profitably used in tuning the relaxation dynamics.

Mechanically activated (milled/alloyed) nano size particles possess altered (reduced [21] or enhanced [22, 23, 24, 25, 26]) magnetic moment in comparison with their corresponding bulk counter parts. It may be mentioned that there is a clear distinction between mechanical alloying and mechanical milling methods in preparation of nanoparticles [27]. In the latter, a bulk material, prepared by other techniques, is milled to reduce the particle

size. Mechanical alloying on the other hand is normally a dry, high energy ball-milling technique that allows production of homogeneous materials in the nano-phase, starting from blended elemental powder (different metal or alloys/compounds) mixtures taken in stoichiometric ratio, required for the preparation of bulk materials. Reduction of magnetization and magnetic order with decreasing particle size in nano size ferrite system is a well established phenomenon [21, 26]. However, enhancement of magnetization and magnetic order, reported here are unique properties of mechanically alloyed nano-particle systems. Site exchange of cations among A and B sites [29, 30], reduction of spin canting at B site [25], and strain induced anisotropy controlled grain boundary effect [26] is thought to play a major role. As yet there is no clear solution of this problem.

Keeping in mind the above scenario we have used a mechanical alloying technique to prepare two systems of $Ni_{0.35}Zn_{0.65}Fe_2O_4$ samples in order to study how, the increasing magnetization with decreasing particle size can affect the stability / relaxation of a nano-magnetic system.

Mechanically alloyed $Ni_{0.35}Zn_{0.65}Fe_2O_4$ nano-particles were synthesized at room temperature with the help of a Fritsch Planetarry Mono Mill pulverisette 6. Iron Oxide (αFe_2O_3) (purity-99.98%), Zinc Oxide (purity-99.98%) and Nickel Oxide (purity-99.99%) have been taken in stoichiometric ratio within an agget bowl of the ball mill grinder. In order to get a homogeneous mixture, the material was ground for 3 hours manually. Zirconium balls of 10 mm in diameter have been used. Ball to mass ratio was 16:1. Grinding experiments have been performed in air with the rotational speed of the Mill at 330 rpm. After each interval of 20 hours a part of the mixture has been taken out for XRD measurements. After 100 hours of milling a single-phase ferrite structure formation has been noticed (labelled as Sample 1). A part of Sample 1 is palletized by pressing it in a steel die at 10 tons / sq. cm. pressure and annealed at 800^0C for 12 hours (labelled as Sample 2).

The morphology, average particle size and crystal structure of both the samples were studied by HR-TEM and X-ray diffraction pattern (by a Phillips diffractometer: model 1710, using Cu-K1 radiation). The x-ray diffraction of the two samples indicates the formation of a single phase, cubic spinel structure (fig.5.1). HR- TE Micrographs (fig.5.2) confirm that spherical nanopanoparticles with average particle size 25 nm and 50 nm have been formed in samples 1 and 2 respectively. The average crystallite size of the sample

measured from the XRD line broadening, using the Scherrer formula[1][32], agrees quite well with that measured from HR-TEM.

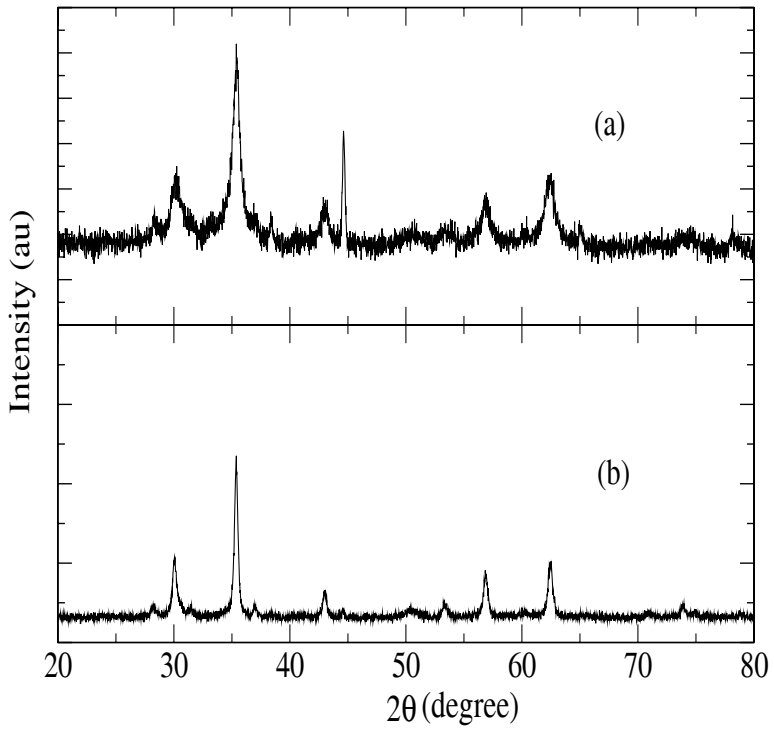

Figure 5.1: X-Ray diffraction pattern of two samples (a)Sample 1 (b) Sample 2

Fig.5.3 depicts the field cooled(FC) and zero field cooled (ZFC) magnetization measurements for samples 1 and 2 in a SQUID magnetometer. In FC technique the sample is first heated to the higest temperature from which it is cooled but in the presence of an external magnetic field H and M(T) is measured along the cooling path. In ZFC measurement, on the other hand, the system is cooled to the lowest temperature in absence of H and M(T) is measured while heating the sample in the presence of H = 100Oe. For a superparamagnetic system the ZFC magnetization curves are expected to show a peak

[1]see chapter 3

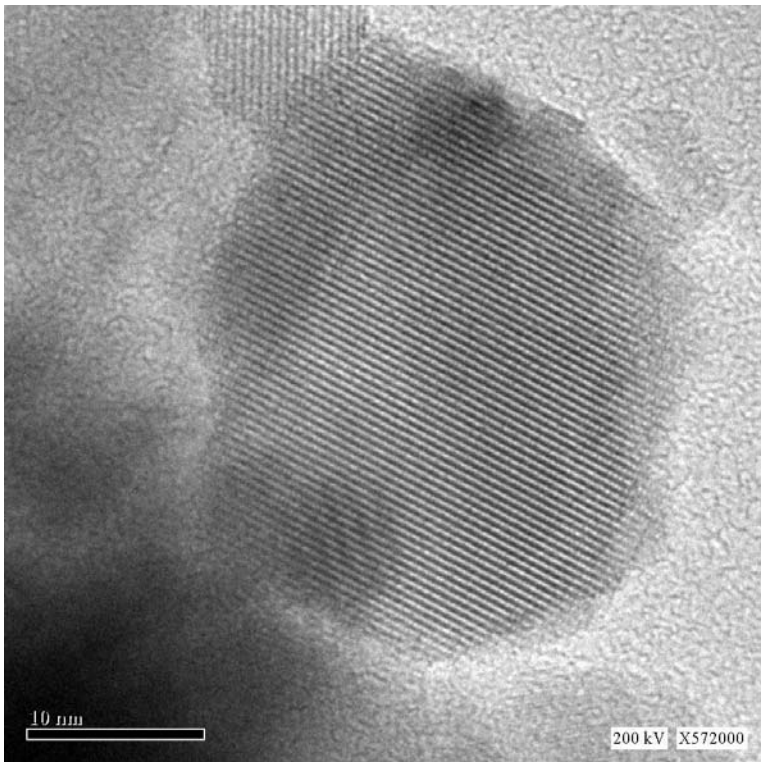

Figure 5.2: High resolution transmission electron micrograph of Sample 1, to study the morphology and to estimate the 'd' value of the crystal planes

corresponding to the average blocking temperature (T_B) of the sample. Our measurement shows that Sample 2 with larger particle size has a higher T_B than that of Sample 1, as expected. The average blocking temperature of Sample 1 is 250 K and that of Sample 2 is 350 K in accordance to the ZFC measurements.

Two surprising points were noticed when we performed temperature-dependent DC M-H measurements (fig.5.4). Firstly we found that Sample 1 with a smaller particle size has a much larger saturation (magnetization at largest applied field) than Sample 2. We also observed that this saturation magnetization of Sample 1 increased much more rapidly in comparison with Sample 2, with decreasing temperature. The second surprising result was that the coercivitty of Sample 1 was higher than that of Sample 2, at all temperatures, in spite of the fact that the former was smaller in size.

Room temperature and low-temperature Mössbauer [33, 34]data are obtained using a CMTE constant acceleration drive (Model- 250) with a 5 m Ci ^{57}Co source in Rh matrix.

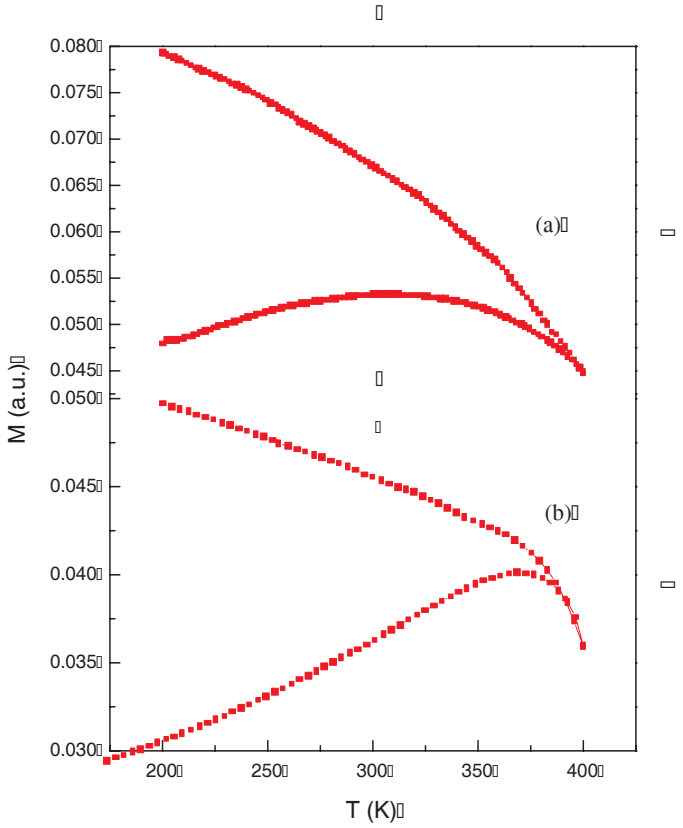

Figure 5.3: Field-Cooled (upper) and Zero Field-Cooled (lower) magnetization curves of (a)Sample 1 and (b)Sample 2 with H=100Oe

The room temperature Mössbauer spectra of Sample 1 and Sample 2 in fig.5.5 are distinctly different. The spectra of Sample 1 is dominated by a doublet [2] having Isomer Shift = 0.31 mm/S, a Quadrupolar Shift = 0.8 mm/S. Though there is a prominent doublet in the spectrum of Sample 2, signature of ferromagnetic ordering is also clear. Crystallites in Sample 1 are small enough so that thermally induced energy fluctuations overcome the anisotropy energy barrier and change the direction of magnetization of nanocrystallites from one easy axis to another. Therefore the presence of only a doublet in the Mössbauer spectrum of Sample 1 indicates superparamagnetic behavior at room temperature. Thus far our results are along the expected lines of 'motional averaging' of spectra due to rapid

[2] see chapter 3

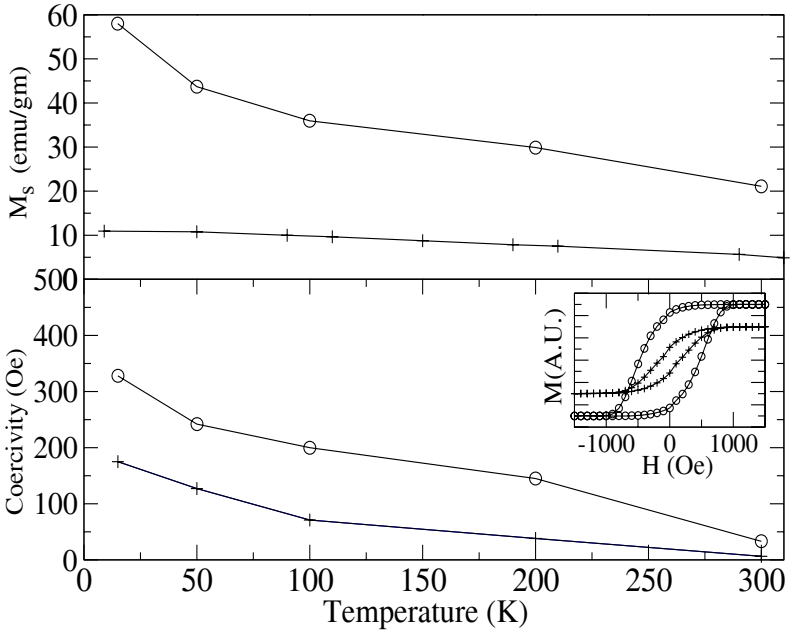

Figure 5.4: figure (a) (Top panel)saturation magnetization of Sample 1 and 2 as function of temperature, figure (b) is corecivity of Sample 1 and 2 as function of temperature. Inset is the simulated DC M-H measurement of Sample 1 and Sample 2. It can be seen that small particle (o) with large saturation magnetization can have larger coercivity than the large particle (+) with small saturation magnetization for same characteristic time scale of measurement.

relaxation, over lower barrier for Sample 1. As the temperature decreases to 21 K, we get the sextet pattern for both the samples, but the line width for Sample 1 is less than that for the Sample 2. This points to an enhancement of magnetic ordering temperature in the smaller sized particle. This observation is consistent with the average hyperfine magnetic field for Sample 1 being greater than the average hyperfine magnetic field for Sample 2, as coroborated below. All these experimental findings lead us to the following model. Let us note that the Sample 1 has a smaller anisotropy barrier (KV_1) than the Sample 2 (KV_2) (where V_1 and V_2 are the volume of sample 1 and sample 2 respectively) because $V_1 < V_2$. But, contrary to the usual case in which the magnetic moment per particle scales up with volume, the magnetic moment and the internal magnetic field as well as

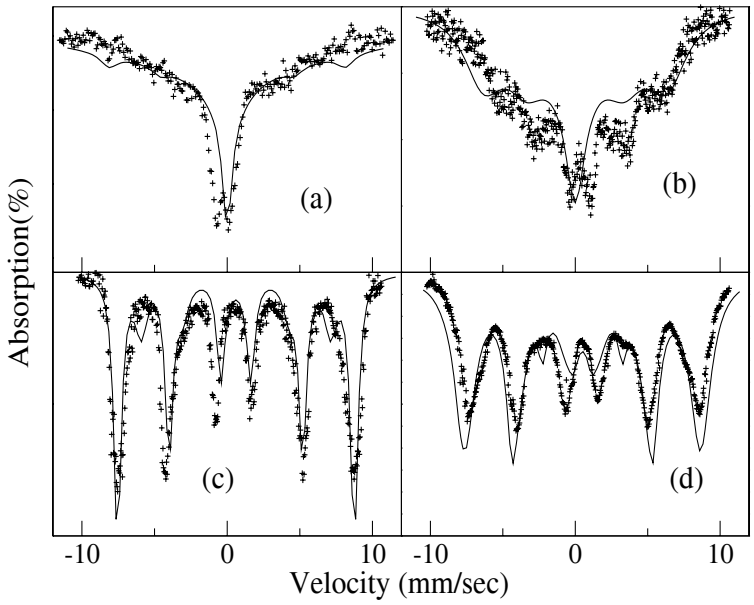

Figure 5.5: Fitted Mössbauer spectra of two samples taken at room temperature and at 21K, using mossbauer line shape equation with a bimodal distribution of particle size. (a)Sample 1 at room temperature (b)Sample 2 at room temperature (c)Sample 1 at 21K and (d)Sample 2 at 21K

the temperature dependence of Sample 1 are found to be much stronger than that of Sample 2. For simplicity in numerical simulation we have assumed that this internal field has a tanh(1/ Temperature) dependence, as in a two state adaptation of our rotational relaxation model [18]. All the observed curves of our experiments can be well explained on the basis of this model.

The M-H curves can be understood in the following way. The remanent magnetization (in most cases a measure of hysteresis) is the magnetization of the system at a time t after the magnetic field is switched off in accordance with M(t) = M(0) exp. (-t/τ), where τ is the relaxation time (τ=τ_0 exp.(KV/k_BT)) and M(0) is the magnetization at the time of switching off the magnetic field. Hence, given a time of measurement (t), a larger remanent magnetization should usually be observed for larger particles if M(0) is the same. However, because of the fact that M(0) of the smaller particle is so much higher

that even with a smaller τ it can give a larger value of M(t). Thus it is not surprising that the smaller particle has a larger coercivity than the larger particle with comparatively low magnetization. We may recall that FC- ZFC measurement yields the standard result that Sample 1 (with smaller energy barrier) has a lower blocking temperature. The coercivity being the standard yardstick for magnetic stability and memory, our central conclusion is therefore that not only the particle size and inter particle interaction but also magnetization of the samples can be properly tuned to change the relaxation dynamics of nano-magnetic systems.

We now try to understand the Mössbauer spectra with the help of above model. Because $V_1 < V_2$, the blocking temperature $T_{B1} < T_{B2}$, as usual. At room temperature Sample 2 yields a small signature of a sextet pattern whereas due to low anisotropy barrier the Sample 1 does not show any such signature. It is well known that application of an external magnetic field can give rise to a six finger pattern even above the normal blocking temperature. Let us assume that the lowest possible temperature ($T_L = 21$ K) of Mössbauer spectroscopic measurement is greater than both T_{B1} and T_{B2} ($T_{B1} < T_{B2}$). Because of the higher internal magnetic field (which is proportional to magnetization) as well as its strong temperature dependence, the blocking temperature of the smaller particle (Sample 1) is shifted above T_L whereas the blocking temperature of Sample 2 remains below T_L. Hence at T_L we have a well resolved sixfinger pattern for Sample 1, but the pattern of Sample 2 is still not well resolved, in spite of the fact that at room temperature Sample 1 has almost a vanishing six finger pattern.

To simulate the experimental curves numerically we assume that our system consists of single domain uniaxal magnetic nanoparticles. For simplicity we also assume that there is no interparticle interaction (like dipolar or exchange) between these nanomagnets. Assuming that the easy axes of all the particles are parallel to each other and parallel to the applied magnetic field (H) the energy is $E|_{H=0}=KV\sin^2\theta$ and $E|_H=KV\sin^2\theta$-MH $\cos\theta$, where θ is the angle between the magnetic moment $\vec{M}$ and the easy axis. To study the dynamics of such a spin system one ordinarily needs to solve the full Fokker-Planck equation for the probability distribution as a function of θ and the time t. But at the high barrier weak noise limit ($KV > k_BT$) this equation goes into a much simpler set of two

state rate equations

$$dn_1/dt = -n_1/\tau_1 + n_2/\tau_2 \tag{5.1}$$

and

$$n_2(t) = n - n_1(t), \tag{5.2}$$

where n_1 and n_2 are the numbers of moments along and opposite to the direction of applied magnetic field (H), with $\tau_i = \tau_0 \exp(E_i|_H/k_B T)$; i=1,2 for i=1, θ=0 and for i=2, $\theta=\pi$ [18]. For Sample 1 we have taken KV/k_B =100 and that for Sample 2 is equal to 500. The particle magnetization of Sample 1 is taken 5 times larger than that of Sample 2. To analyse the Mössbauer spectra we have used the line shape formula [3] as a function of frequency ω, with a bimodal particle distribution [35],

$$\begin{aligned} I(\omega) &= \frac{1}{\pi} Re \sum\nolimits_{m_0 m_1} |\langle I_0 m_0|A|I_1 m_1\rangle|^2 \\ \times & \sum\nolimits^2_{i=1} V_i[(-i\omega + \frac{\Gamma}{2}) + \frac{{\mu_N}^2 {h_0}^{i^2} (g_0 m_0 - g_1 m_1)^{-2}}{(-i\omega + \frac{\Gamma}{2}) + \lambda(V^i)/2}]. \end{aligned} \tag{5.3}$$

Here we have taken the hyperfine field (h_0) of smaller particle 1.14 times larger than that of the larger particle. The ratio of small to large particle is taken as 75:25 and 20:80 for Sample 1 and Sample 2 respectively.

In conclusion, two samples of $Ni_{0.35}Zn_{0.65}Fe_2O_4$ nano particles have been prepared by mechanically activated (alloyed) method. X-Ray diffraction suggests that single phase $Ni_{0.35}Zn_{0.65}Fe_2O_4$ nanoparticles have been prepared. The average particle size estimated from the broadening of X-Ray diffraction peak are 25nm and 50nm respectively for Sample 1 and Sample 2. HR-TEM micrograph has been used to analyse the particle size distribution and morphology of the samples. The micrograph suggests that spherical nanoparticles with log-normal distribution in the particle size have been prepared. The crystallographic 'd' values measured from this micrograph agree well with the bulk value in $Ni_{0.35}Zn_{0.65}Fe_2O_4$. The DC M-H measurement show that samples prepared by this method can have higher magnetization in smaller nanoparticles than in larger particles. DC magnetic measurement also suggests unusual behavior in coercivity versus temperature: Sample 1 has larger coercivity at all measured temperatures than Sample 2 inspite of smaller average particle size. In Mössbauer spectroscopy we have seen that at room

[3] see chapter 3

temperature Sample 1 has a dominant singlet compared to Sample 2 where we have a signature of sextet even at room temperature. The situation becomes completely opposite at the lowest measured temperature (at 20K), where we see a well resolved sextet in Sample 1 whereas the six finger pattern of Sample 2 is still not well resolved. Keeping this in mind we suggest a model where in we show that the enhancement of magnetization with decreasing particle size leads to larger stability in smaller particle in certain measurements. We have further used computer simulations to validate our model. Finally we can state that not only the particle volume and interparticle interaction but also the **magnetization** can be used to tune the stability of nano-magnetic particles. The latter attribute has important applications in storage media.

Bibliography

[1] S.H. Sun, *et-al*, Science **287**, 1989 (2000).

[2] R.H. Kodama, J. Magn. Magn. Mater., **200**, 359 (1999).

[3] J. Frenkel and J. Dorfman, Nature (London) **126**, 274 (1930); C. Kittel, Phys. Rev. **70**, 965 (1946).

[4] C. P. Bean and J. D. Livingstone, J. Appl. Phys. **30**, 1205 (1959); I. S. Jacobs and C. P. Bean, in Magnetism, vol. III, (G. T. Rado and H. Suhl, eds.) Academic Press, New York, 1963.

[5] L. Néel, Ann. Geophys. **5**, 99 (1949); Adv. Phys. **4**, 191 (1955).

[6] A.N. Goldstein, *Hand Book of Nanophase Materials* (New York:Marcel Dekker Inc.)(1997).

[7] *Magnetic Properties of Fine Particles*, edited by J. L. Dormann and D. Fiorani (North-Holland, Amsterdam, 1992).

[8] K. M. Unruh and C. L. Chein, *Nanomaterials: Synthesis, Properties and Applications*, eds., A .S. Edelstein and R. C. Cammarata (Bristol: Institute of Physics).

[9] *Physical Principles of Magnetism*, A.H.Morrish, John Wiley,New York,1965.

[10] Steen Mϕrup and Elisabeth Tronc, Phys. Rev. Lett. **72**,3278(1994).

[11] E. P. Wohlfarth, J.Phys.**F10**,L241(1980).

[12] R. Street and J. C. Woolley, Proc. Phys. Soc. London, Sec A **62**, 562 1949. Also reviewed in S. Dattagupta, *Relaxation Phenomena in Condensed Matter Physics, Chapter XV*, Academic Press, Orlando(1987).

[13] P. E. Jönsson, Adv. Chem. Phys., 128, 191-248 (2004).

[14] M. F. Hansen, P. E. Jönsson, P. Nordblad and P. Svedlindh, J. Phys.: Condens. Matter 14, 4901 (2002)

[15] C. Frandsen, C. W. Ostenfeld, M. Xu, C. S. Jacobsen, L. Keller, K. Lefmann, and S. Morup Phys. Rev. B 70, 134416 (2004)

[16] Franz Bdker, Mikkel F. Hansen, Christian Bender Koch, Kim Lefmann, and Steen Morup Phys. Rev. B 61, 6826 (2000)

[17] Mikkel F. Hansen, Franz Bdker, Steen Morup, Kim Lefmann, Kurt N. Clausen, and Per-Anker Lindgrd Phys. Rev. Lett. 79, 4910 (1997)

[18] S. Chakraverty, M. Bandyopadhyay, S. Chatterjee, S. Dattagupta, A. Frydman, S. Sengupta, and P. A. Sreeram Phys. Rev. B 71, 054401 (2005)

[19] S. Chakraverty, A. Frydman, V.G. Pol, S. V. Pol, A. Gedanken, cond-mat/0505054

[20] Y. Shi and J. Ding, J. Appl. Phys, 90, 4078 (2001).

[21] D. Lin, A.C. Nunes, C. F. Majkrzak and A. E. Brekwitz, J. Magn. Magn. Mat, 145, 343 (1995).

[22] V. Sepelak et al. J. Magn. Magn. Mat., 257, 357 (2003) and references therein.

[23] S. A. Oliver, V. G. Harris, H. H. Hamdeh and J. C. Ho, Appl. Phys. Lett. , 76, 2761 (2000).

[24] J. Z. Jiang, G. F. Goya and H. R. Rechenberg, J. Phys C, 11, 4063 (1999).

[25] R. N. Bhowmik, R. Ranganathan, S. Sarkar, C. Bansal and R. Nagarajan, Phys. Rev. B 68, 134433 (2003). 15.R. N. Bhowmik, R. Ranganathan, R. Nagarajan, B. Ghosh and S. Kumar, Phys. Rev. B 72, 094405 (2005).

[26] J. M. D. Coey, Phys. Rev. Lett. 27, 1140 (1971).

[27] C. Suryanarayana, Progess in Material Science , 46, 1-184 (2001).

[28] R. H. Kodama, A. E. Barkowitz, E. J. McNiff and S. Foner, Phys. Rev. Lett, 77, 394 (1996).

[29] H. H. Hamdeh et al. J Appl. Phys, 81, 1851 (1997).

[30] V. A. M. Brabers, Phys. Rev. Lett, 68, 3113 (1992).

[31] C. Caizer and M. Stefanescu,, J. Phys D, 35, 3035 (2002).

[32] B. D. Cullity, *Elements of X-ray Diffraction*(1978). B. Ghosh, Ph.D. dissertation (2006), unpublished

[33] A large body of work on Mössbauer effect in single domain magnetic particles has been carried out by S. Mϕrup and his group. A recent reference is: M. F. Hansen, C. B. Koch, and S. Mϕrup, Phys. Rev. B **62**, 1124(2000).

[34] S. Dattagupta in Mössbauer Effect: Application to Physics, Chemistry and Biology, (B. V. Thosar, P. K. Iyengar, J. K. Srivastava and S. C. Bhargava, eds.) Elsevier, Amsterdam, 1983.

[35] S. Dattagupta, in *Mössbauer Spectroscopy in Perspectives* (F. J. Berry and D. P. E. Dickson, eds.) Cambridge University Press, London and New York, 1986; also in Hyperfine Interaction **49**, 253 (1989).

Chapter 6

Magnetic coding in systems of nanomagnetic particles

Magnetic nanoparticles are gaining increasing interest due to their vast technological potential as magnetic based nano-electronic devices [1, 2, 3, 4, 5, 6]. One of the exotic phenomena observed in systems of single domain magnetic nano-particles is a history-dependent magnetic memory in the DC magnetization of the system as a function of temperature [7, 9, 10, 11]. Starting at high temperature, the system is steadily cooled in a small magnetic field, H, and the magnetization, M, measured as a function of temperature. At intermediate temperatures the cooling is arrested and the field switched off for a few hours before being restored. When the system is heated from the lowest temperature, M(T) shows wiggles at all T steps where H was previously switched off, apparently keeping a memory of the temperature arrests.

Two explanations have been suggested for such behavior. The first attributes the history dependent M(T) to aging and concomitant memory effects in a spin glass phase [7]. This explanation hinges on the frustration of the magnetic moments of the particles due to dipole-dipole interactions, giving rise to deep energy valleys trapping the system for extended times [8].

An alternative origin for the memory effects is based on a broad distribution of particle size [9, 10, 11]. The polydispersity of the particle volumes leads to a wide distribution of blocking temperatures, T_B. The memory effects are a consequence of the fact that the system is arrested at temperatures which lie between blocking temperatures of different sized particles.

In this chapter we present an experimental study of nano-magnetic systems and show that the effect of a sudden *increase* of magnetic field can also be stored in the system as long as the field is not too high. Using numerical simulations we show that this behavior is consistent with a wide distribution of particle sizes having different blocking temperatures and discuss possible applications of this effect

The results presented in this chapter were obtained on nanomagnetic systems of $Ni_{0.35}Zn_{0.65}Fe_2O_4$. However similar results were obtained for systems of $NiFe_2O_4$ particles embedded in a SiO_2 matrix [9] and on Ni particles embedded in an Au matrix (Preparation described in [12]). The $Ni_{0.35}Zn_{0.65}Fe_2O_4$ particles were prepared by mechanical alloying processes utilizing Fritsch Planetary Mono Mill Pulverisette 6. The mean crystalline size estimated from powder XRD analysis was 27 nm. Figure 1 depicts a TEM micrograph of such a sample, exhibiting particles with sizes ranging from 10nm to 100 nm.

Our experiments were carried out in accordance with the following cooling and heating protocol. At T=300K a magnetic field of H=50Oe was applied and the magnetization (M) measured in a SQUID. Keeping the field on, the temperature(T) was lowered continuously at a rate of 2K per minute to $T_1 < 300K$ and then the field was either switched off or increased to 400Oe and arrested at this state for 4 hours before a 50Oe field was restored. The sample was than cooled to $T_2 < T_1$ after which the field was changed again while arresting the system for 4 hours. Finally, the field was changed back to 50Oe and the sample was cooled to a minimal temperature of 10K. The system was then heated back to room temperature in the presence of H=50Oe and the heating profile of M(T) was monitored. Results for different changes of magnetic field are summarized in fig. 6.2. It is seen that the heating M(T) curve detects both decreasing and increasing magnetic field changes which occur during the cooling protocol. Hence, it is possible to code binary numbers like 0 and 1 by defining the "H decrease" as 0 and "H increase" as 1. These can be decoded by heating the system at a constant rate in presence of a constant magnetic field .

The ability to store the information of many changes is restricted to small magnetic fields. If a field above a critical value, H* is applied, it erases the memory effects of the smaller H changes. An example is shown in figure 6.3 where applying a magnetic field of

800Oe results in erasing the fingerprint of a previous magnetic field change.

The observed behavior is naturally understood on the basis of the wide size distribution of particles. Due to the polydispersity, the system contains a wide distribution blocking temperatures, T_B. Thus, for each arrested temperature some of the particles are superparamagnetic while others are blocked. An increase or decrease of magnetic field will be imprinted in large grains but not in small ones since upon restoring the field (after arrestment), the small particles will show facile response while the large ones will not. Further cooling of the sample causes the magnetization (M) in the small particles to increase with temperature while M in the large one will remain almost constant. As T is increased again, M for small particles decreases while for large particles it initially increases before dropping off at $T > T_B$. Due to the wide size distribution, any arresting temperature will correspond to a T_B of some particles, hence, the M(T) during heating will show wiggles at the cooling arrested temperatures, thus mimicking the cooling curve and "remembering" the arrested temperatures. This explanation is not related to complex spin-glass type interactions and applies for non-interacting single-domain magnetic particles.

The above reasoning applies only if the H is not too large. If the applied field is large enough to flip all (or most) of the particles, it will erase the previous imprinted memory. In order to understand this we consider, for simplicity a system of magnetic nanoparticles having three distinct volumes $V_1 < V_2 < V_3$ corresponding to three blocking temperatures $T_{B1} < T_{B2} < T_{B3}$. During the cooling process the system is arrested at two temperatures, T_1 and T_2 so that $T_{B1} < T_1 < T_{B2} < T_2 < T_{B3}$. Arresting the system at T_2 and changing the magnetic field causes the signature of the change to be imprinted only in the largest particles, V_3. Further cooling the sample does not cause magnetic changes in these particles which are blocked in this temperature range, neither does a mild magnetic field change at T_1 which will give rise to a memory sign imprinted in V_2 particles. However, if at T_1, the applied magnetic field is large enough to flip the spins of V_3 that were blocked at T_2, the magnetic state of the large particles will change even at temperatures well below their blocking temperature. In such a case, the memory imprinted at T_2, is erased.

In order to simulate the coding curve we considered a system of magnetic nanoparticles having a tetramodal distribution (four distinct particle sizes). We used a two state rate

equation assuming the anisotropy energy is large enough than the thermal fluctuation to be in Kramers regime. For simplicity we also assumed that the magnetic field is applied along the direction of easy axis of the nanoparticles, so there is no moment rotation but only magnetic orientation flip. Fig. 6.4 shows the results of our simulation for two cases of cooling the sample at a field H, switching the magnetic field off at T=60K and applying a magnetic field larger than H at T=20K. In the first case the applied field is 2H while in the second it is 5H. It is seen that for the mildly applied magnetic field case the heating curve shows magnetization "wiggles" in accordance with the field changes during the cooling process. These are very similar to the experimental results. Applying a large field (bottom panel of fig. 6.4), on the other hand, results in the erasing of the signature of the field switch off at 60K.

The observed effect can have possible application in studying the spatial or temporal variation of magnetic state of a magnetic surface. To study the spacial variation the poly dispersed nano-magnetic sample (PDNM) should move over the surface. During its scan its temperature will be decreased at a constant rate. The scan will end at the lowest temperature assigned to the PDNM sample. After the end of the scan the PDNM will be heated at a constant rate to decode the recorded magnetic data as a function of temperature, which in turn will give the spacial distribution of the magnetic state of the surface. The ability to easily produce very small samples can result in very high spacial resolution. a similar algorithm can be used in case of temporal variation, in which the PDNM should be kept fixed at a point and the variation of the magnetic state of the surface as a function of time will be recorded. The sensitivity of the memory device (PDNM) can be increased by increasing the magnetization of the nano-magnets. The resolution can be improved by properly choosing the relaxation times of the nano-particles and their distribution in the sample.

In conclusion, we have demonstrated that a nanomagnetic particle system can be used to encode a sudden increase or decrease of magnetic field, while cooling the system. The information can be decoded by measuring the M(H) curve during heating. The memory is erased if a large magnetic field is applied. This behavior can be explained as resulting from the wide distribution of particle volumes, without the need of complicated spin-glass type interactions, demonstrating that the lack of particle uniformity can lead to exciting

and exotic magnetic effects.

Bibliography

[1] A.N.Goldstein, *Hand Book of Nanophase Materials*, New York:Marcel Dekker Inc. (1997).

[2] R.H. Kodama, J. Magn. Magn. Mater., **200**, 359 (1999).

[3] *Magnetic Properties of Fine Particles*, edited by J.L.Dormann and D.Fiorani, North-Holland, Amsterdam (1992).

[4] K.M.Unruh and C.L.Chien, *Nanomaterials:Synthesis,Properties and Applications* edited by A.S.Edelstein and R.C.Cammarata, Bristol: Institute of Physics (1996).

[5] I.S.Jacobs and C.P.Bean in *Magnetism III* (eds.) G.T.Rado and H.Suhl, (New York: Academic)(1963).

[6] *Physical principles of Magnetism*, A.H. Morrish, John Wiley, New York, 1965.

[7] Y.Sun, M.B.Salamon, K.Garnier and R.S.Averback, Phys. Rev. Lett. **91**,167206(2003).

[8] A.P. Young, Spin Glasses and Random Fields, eds., Wo rld Scientific, Singapore (1987).

[9] S. chakraverty, M. Bandyopadhyay, S. Chatterjee, S. Dattagupta, A. Frydman, S. Sengupta, and P. A. Sreeram et-al, Phys. Rev. **B71**, 054401 (2005).

[10] R.K. Zheng and X.X. Zhang, cond-mat/0403368.

[11] M.Sasaki, P.E.Jonsson, H.Takayama and P.Nordblad, Phys. Rev. Lett. **93**, 139701 (2004).

[12] S Chakraverty, A. Frydman, V.G. Pol, S.V. Pol and A. Gedanken, cond-mat/0505054.

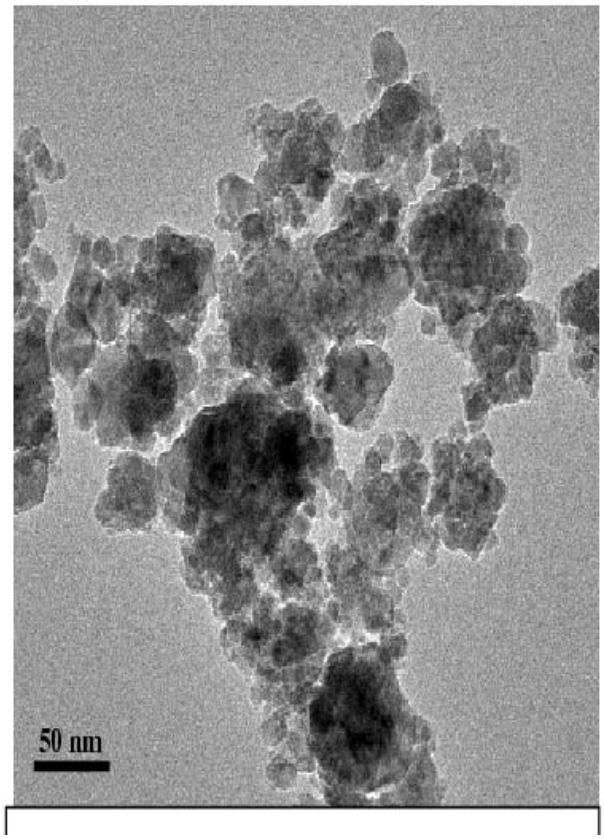

Figure 6.1: micrographs of $Ni_{0.35}Zn_{0.65}Fe_2O_4$ particles with diameters ranging from 10 to 100 nm..

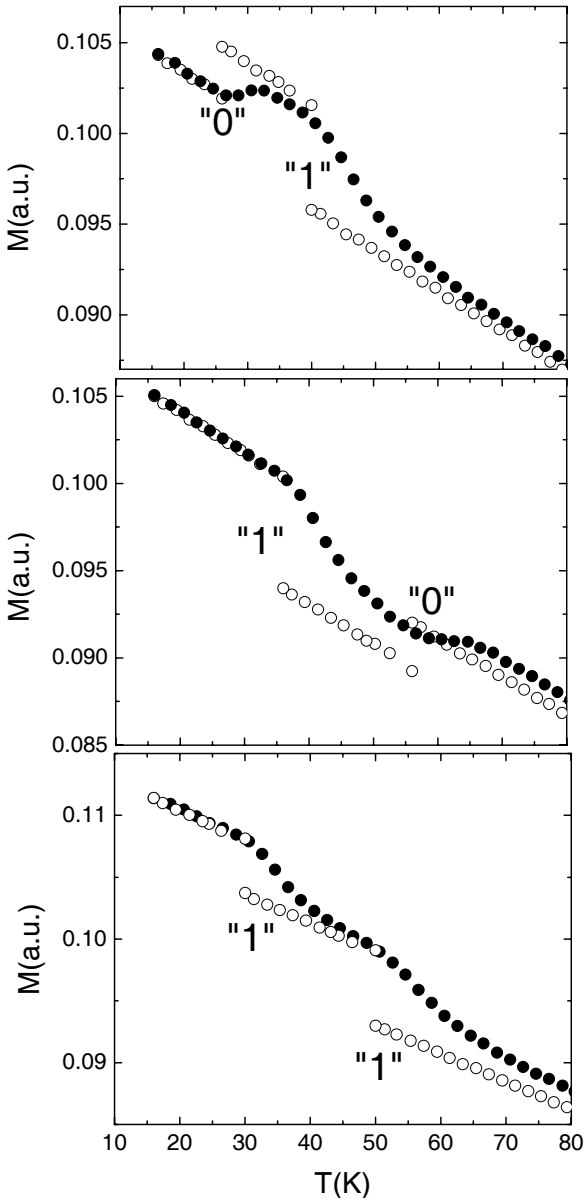

Figure 6.2: M(T) curves while cooling (open circle) and heating (solid circle) of the nanomagnetic particle systems at 50Oe. During the cooling process the following magnetic fields changes were performed: At 40K a 400Oe is applied and at 24K the field is switched off (top panel), at 50K the field is switched off and at 30K a 400Oe field is applied (middle panel), a 400Oe field is applied both at 50K and at 30K (bottom panel). Note that the heating curves show different "wiggles" for the increase or decrease of magnetic field during the cooling process.

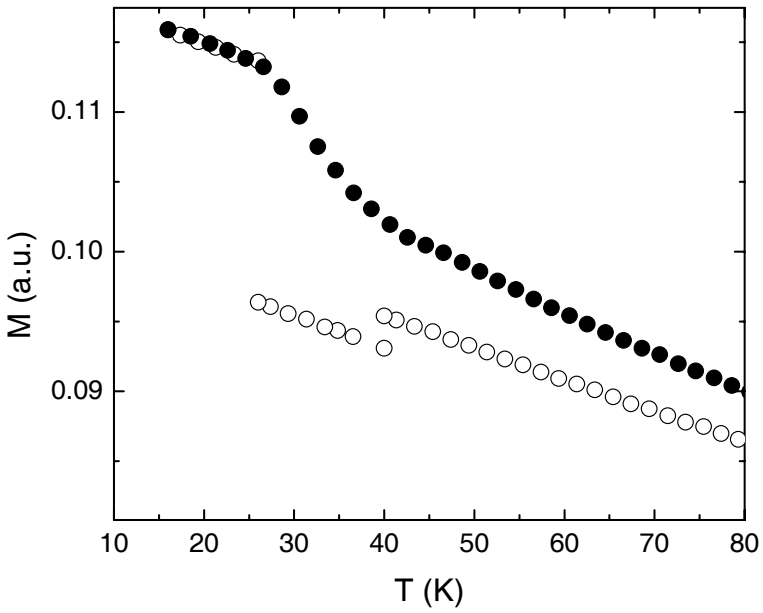

Figure 6.3: M(T) curves for the cooling (open circle) and heating cycle (solid circle) while switching off the field at 40K and applying a *800Oe* field at 24 K. In this case, the signature of the field switching off at 40K is erased from the heating curve.

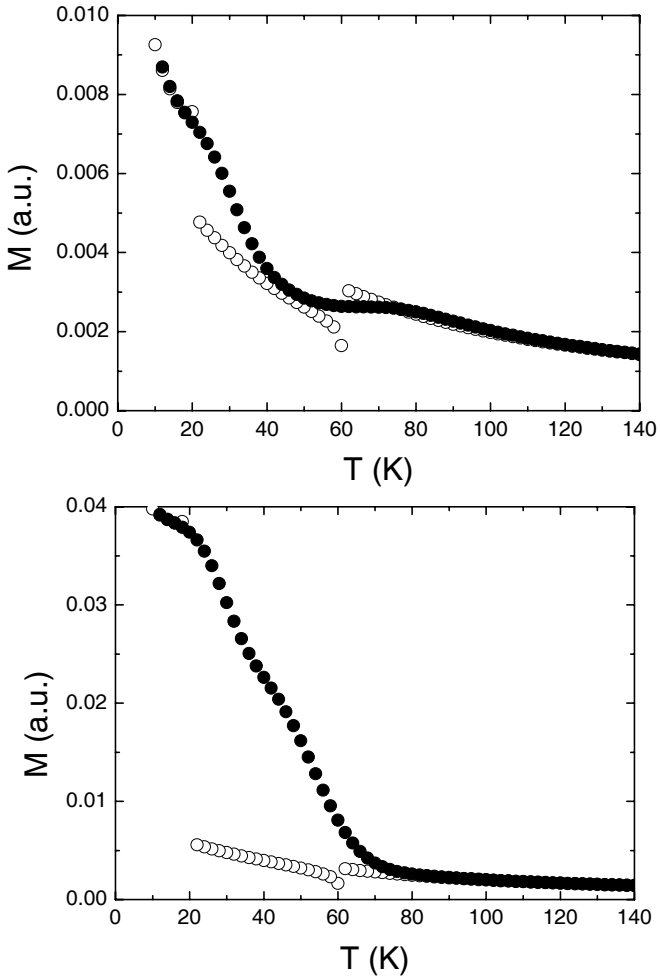

Figure 6.4: Results of our simulations for a system in which the sample was cooled (open circle) at a magnetic field, H. At T=60K the field is switched off and the temperature of the system is arrested before restore the field H and at 20K a field of 2H (top panel) or 5H (bottom panel) is applied. Note that the application of a large field erases the effect of the previous magnetic field switching off. The solid circles in the figure are the magnetization during heating cycle.